Saturated fatty acid-Coenzyme A supplementation restores neuronal energy levels, synaptic function, and protein homeostasis in hereditary spastic paraplegia

Saber H. Saber[1,2], Nyakuoy Yak[1,2], Xuan Ling Hilary Yong[2], Siyuan Lu[1], Tobias Binder[1], Reshinthine Purushothaman[1], Arnaud Gaudin[2], Jeffrey Harmer[1,3], Gert Hoy Talbo[1], Ashley J van Waardenberg[4], Victor Anggono[2], Giuseppe Balistreri[5] and Merja Joensuu[1,2,*]

[1] Australian Institute for Bioengineering and Nanotechnology, The University of Queensland, Brisbane, Queensland, Australia
[2] Queensland Brain Institute, The University of Queensland, Brisbane, Queensland, Australia
[3] Centre for Advanced Imaging, The University of Queensland, Brisbane, Queensland, Australia
[4] i-Synapse, Cairns, Queensland, Australia
[5] Department of Virology, Faculty of Medicine, University of Helsinki, Helsinki, Finland
* Correspondence m.joensuu@uq.edu.au

Abstract

Hereditary Spastic Paraplegia (HSP) type 54 is a complex childhood autosomal recessive neurodegenerative disorder characterized by impairments in both neuromuscular and cognitive functions. This condition arises from mutations in the *DDHD2* gene, which encodes for the phospholipase A1 enzyme DDHD2. Previous research has indicated that loss of *DDHD2* results in lipid droplet accumulation in the brain, progressive apoptosis of motor neurons in the spinal cord, a reduction in cardiolipin content, and an increase in reactive oxygen species. However, the precise underlying mechanisms of HSP54 remains unclear. Our recent study demonstrated a robust increase in saturated free fatty acids (sFFAs), particularly myristic acid, during neuronal stimulation and memory acquisition *in vivo* in the brains of mice and *in vitro* in primary neurons. This activity-dependent increase of sFFAs was blocked in *DDHD2* knockout mice (*DDHD2*$^{-/-}$), suggesting that disturbed production of sFFAs underlies the neuronal pathology of HSP54. Here, using electron microscopy (EM) and live-cell confocal imaging, mass spectrometry and proteomics, electric field stimulation, as well as fluorometric and mitochondrial function assays in cultured primary neurons, we discovered that loss of DDHD2 leads to reduced levels of acetyl-coenzyme A (CoA) and ATP. Additionally, DDHD2 deficiency results in impaired respiratory function, altered mitochondrial morphology and distribution, a significant defect in synaptic vesicle recycling with an accumulation of large bulk endosomes in the presynapses, as well as an imbalance in global protein homeostasis. Our study further reveals that the combined administration of myristic acid and CoA (Myr-CoA) fully rescues mitochondrial function and ATP production within 48 hours. This intervention also leads to a marked restoration of neuronal protein homeostasis, providing the first demonstration of a potential combinatory therapeutic intervention for HSP54. Our findings demonstrate that the sFFAs released by the activity of DDHD2 play a central role in maintaining neuronal energy levels, synaptic function, and protein balance. The requirement for DDHD2 lipase activity in these processes can, therefore, be bypassed by supplementation of a preconjugated Myr-CoA.

Keywords: Hereditary Spastic Paraplegia type 54, DDHD2, myristic acid, presynapse, mitochondria, endocytosis, saturated fatty acid

Introduction

Hereditary spastic paraplegias (HSP) are a group of inherited neurodegenerative disorders characterized by spasticity and weakness in the lower extremities. More than 80 genetic types of HSPs have been identified, affecting a multitude of cellular processes such as intracellular membrane trafficking, lipid metabolism, mitochondrial function, and myelin formation[1-5]. HSP type 54 (HSP54) is a rare, early childhood onset hereditary neurodegenerative disorder that is characterized by progressive brain abnormalities on cerebral imaging, thin corpus callosum, white-matter abnormalities, short stature, delayed psychomotor development and intellectual disability[6-9]. It is caused by mutations in the *DDHD2* gene, encoding for a mammalian intracellular phospholipase A1[10], which cleaves the acyl ester bond at the *sn-1* positions of phospholipid glycerol moieties and of triglycerides. DDHD2 enzymatic activity generates saturated free fatty acids (sFFAs) and 2-acyl-lysophospholipids[11-13], as well as consumes triglycerides from the lipid droplets[14,15]. All identified mutations affect the DDHD domain of the protein, which harbors its phospholipase catalytic activity. Consistent with DDHD2's function in lipid metabolism and its role in the central nervous system, the accumulation of lipids droplets in human brains[10] and in mouse neurons have been reported following the loss of DDHD2 function[14]. We and others have demonstrated that DDHD2 is distributed throughout the neuron, including organelles of the secretory pathway and nerve terminals and to be involved in membrane trafficking[13,16-19]. However, to date, the mechanisms by which *DDHD2* gene mutations cause HSP54 are not well understood.

We recently discovered that synaptic activity induces elevation in the levels of sFFAs, particularly myristic and palmitic acid, both in neuronal cultures *in vitro* and in wildtype C57BL6/J mice *in vivo*[13]. In contrast, *DDHD2* knockout mice (*DDHD2*$^{-/-}$), that display gradual decline in cognitive and motor neuron function, were unable to upregulate the sFFAs in the brain activity-dependently[13]. We therefore hypothesize that the disturbance of sFFA levels significantly contribute to the neuropathology observed in *DDHD2*$^{-/-}$ mice. Given that sFFAs, such as myristic acid, can be used as an energy source, as a substrate for protein lipidation (i.e. N-terminal myristoylation), and have a role in regulating membrane fluidity, here we investigated whether loss of DDHD2 function affects neuronal energy levels, protein homeostasis and synaptic membrane trafficking.

We discovered that deletion of *DDHD2* leads to a significant reduction in the levels of acetyl-coenzyme A (CoA) in mouse brain tissues, which is an important cofactor molecule required for a variety of cellular functions, including protein lipidation (e.g. N-myristoylation and S-palmitoylation), Krebs cycle, fatty acid metabolism, acetylcholine synthesis and acetylation[20]. Moreover, the loss of DDHD2 impairs mitochondrial respiratory function and leads to a decreased production of ATP, altered mitochondrial ultrastructure and distribution, and a substantial defect in synaptic vesicle recycling, marked by an accumulation of large bulk endosomes, alongside with an imbalance in global protein homeostasis. We further demonstrate, that the externally applied myristic acid in combination with CoA (Myr-CoA) fully rescues the mitochondrial function and ATP production within 48 hours and leads to a marked restoration of presynaptic vesicle recycling, and neuronal protein homeostasis, identifying a potential therapeutic intervention for HSP54.

Results

Loss of DDHD2 leads to an increase in somatodendritic mitochondria size and an accumulation of mitochondria in the presynapses

Mitochondria play a pivotal role in various cellular processes including ATP (Adenosine triphosphate) production, maintenance of intracellular Ca^{2+} balance, generation of reactive oxygen species (ROS), and regulation of apoptosis. Given their elevated energy requirements, neurons are especially sensitive to mitochondrial dysfunction, which is emerging as one of the pathological processes in neurological

disorders[21]. A potential connection between lipid metabolism in mitochondria and the HSPs has been established[22]. DDHD2 has been shown to have a protective role for mitochondrial integrity, while the knockout of *DDHD2* in mice has been shown to lead to an increase in ROS production[23]. *DDHD1*, which encodes for another intracellular phospholipase A1 isoenzyme, has been reported to affect mitochondrial morphology in an activity-dependent manner[24] and, when mutated, to cause HSP28[25]. Furthermore, lipid-modifying enzymes, including phospholipases and lipid phosphatases, may play a role in orchestrating local lipid composition to spatially and temporally coordinate a balance between fusion and fission, thereby influencing mitochondrial morphology[26].

To study the mitochondrial ultrastructure in more detail in *DDHD2*$^{-/-}$ mice, we first performed electron microscopy (EM) analysis in cultured wildtype (C57BL6/J) control and *DDHD2*$^{-/-}$ hippocampal neurons at DIV21-22 (days in vitro) (Fig. 1A). By quantifying the sectional area of the mitochondria from EM thin sections (80-90 nm), we found significantly enlarged mitochondria in the somatodendritic compartment in *DDHD2*$^{-/-}$ neurons compared to wildtype, while no changes were observed in the average mitochondrial size in axons or presynapses (Fig. 1B). Together with our earlier demonstration of perturbed sFFA balance, in particular myristic acid, in the brain of *DDHD2*$^{-/-}$ mice[13], these results suggest that sFFAs may play a role in the structural integrity of mitochondria.

Myristic acid can be conjugated to the N-terminus of a subset of cellular proteins, allowing them to bind biological membranes (i.e. N-myristoylation). An acute pharmacological inhibition of N-myristoyltransferases (NMT) 1 and 2 with the small molecule IMP-1088[27] for 16 hours exacerbated the enlarged mitochondrial phenotype, suggesting that myristic acid and protein N-myristoylation may play a key role in this process (Fig. 1A, 1B). While the axonal and presynaptic mitochondrial size was not affected by the loss of DDHD2, we observed a significant accumulation of mitochondria in resting (non-stimulated) *DDHD2*$^{-/-}$ presynapses compared to control, which was further amplified following a 50 Hz electrical stimulation (6 seconds, followed by 10 minute incubation before fixation and processing for EM) (Fig. 1C), indicating loss of DDHD2 function in neurons leads to a mitochondrial distribution defect. Together, these results indicate that loss of DDHD2 function, which leads to perturbed sFFA balance[13], and the acute inhibition of N-myristoylation, similarly lead to aberrant mitochondrial structure and distribution in neurons. Supporting these findings, live cell imaging of mitochondria in human A549 cells using MitoTracker, revealed that inhibition of protein N-myristylation with 1 μM IMP-1088 for 48 hours leads to an enlargement of mitochondrial size, at the expense of the overall mitochondrial number (Fig. 1D-F). The enlargement of mitochondria could be envisioned to be caused by a dysregulation of mitochondrial fusion/fission, a process regulated by structural proteins, some of which are S-palmitoylated and N-myristoylated[28-30].

Decreased levels of mitochondrial respiration, CoA, and ATP in *DDHD2*$^{-/-}$ neurons are fully restored by myristic acid – CoA supplementation

While the origins of neurodegenerative diseases remain elusive, numerous proposed mechanisms and compelling evidence underscore the crucial role of mitochondrial dysfunction in their pathogenesis[31]. Aberrant accumulation of damaged mitochondria in the presynapses has been suggested as a prominent feature in both familial and sporadic Alzheimer's disease[32-35]. Following our finding of mitochondrial accumulation in the presynapses (Fig. 1C), we next studied how the loss of DDHD2 function affected the mitochondrial function. Using a fluorometric acetyl coenzyme A assay, we observed a significant decrease in the CoA levels in *DDHD2*$^{-/-}$ brain tissues compared to control (Fig. 2A). CoA is an essential cofactor necessary for not only the utilization of sFFAs as a fuel for energy production in mitochondria, but also for the lipidation of proteins (N-myristoylation and S-palmitoylation), Krebs cycle, triglycerides and acetylcholine synthesis[20].

Glycolysis and oxidative phosphorylation are the two major energy-producing pathways in the cell. Most cells possess the ability to switch between these two pathways, thereby adapting to changes in

their environment. Neurons have long been considered to use almost solely glucose as their energy source. To test if the loss of function of DDHD2 lipase activity would affect neuronal mitochondrial function and energy levels, even in the presence of glucose, we assessed mitochondrial function using Seahorse Cell Mito Stress assay in cultured C57BL6/J and *DDHD2*$^{-/-}$ neurons. In this assay, successive injections of small molecule inhibitors oligomycin, carbonyl cyanide-4-(trifluoromethoxy) phenylhydrazone (FCCP), and rotenone/antimycin (Rot/AA) are performed (Fig. 2B). The measured oxygen consumption rate (OCR) serves a direct readout for the basal mitochondrial respiration activity of the cells. The introduction of oligomycin, which inhibits the ATP synthase complex, results in a decrease in OCR. The extent of this reduction informs on the oxygen consumption allocated to ATP production (ATP turnover). FCCP enhances mitochondrial respiration by disrupting the proton gradient between the intermembrane space and the mitochondrial matrix. The introduction of FCCP, which mimics a physiological "energy demand' by prompting the respiratory chain to operate at its outmost capacity, leads to the rapid oxidation of substrates (including sugars, fats and amino acids) to meet the metabolic challenge. After FCCP treatment, cells reach their maximal oxygen consumption, representing the neurons' highest achievable respiration rate during stimulation. The highest OCR value attained represents the maximum respiratory capacity, and the disparity between this peak and basal respiration defines the spare respiratory capacity. The third mediator is a mixture of Rot/AA (i.e. a complex I and III inhibitors, respectively), which inhibit the electron transport chain complex and shut down mitochondrial respiration. The residual OCR often observed in these experiments is due to non-mitochondrial reactions occurring within the cells. We observed a significant OCR reduction in *DDHD2*$^{-/-}$ neurons (Fig. 2B, green line) compared to control neurons (Fig. 2B, blue line). Statistical analysis for each of the respiration stages described in Figure 2B confirmed that compared to control neurons, *DDHD2*$^{-/-}$ neurons displayed significantly lower basal respiration (Fig. 2C), maximal respiration (Fig. 2D), non-mitochondrial oxygen consumption (Fig. 2F), mitochondrial mass (Fig. 2F) and ATP levels (Fig. 2G).

We have previously shown that loss of DDHD2 leads to a significant decrease in activity-dependent upregulation of sFFAs, in particular myristic acid[13]. To be utilized as fuel in ß-oxidation, as a substrate for protein lipidation, or for the synthesis of complex lipids, sFFA must be first conjugated with CoA, the levels of which we found to be significantly lower in *DDHD2*$^{-/-}$ neurons. In addition, the coupling of sFFA with CoA requires ATP, which was also less abundant in cells devoid of DDHD2. To attempt rescuing the identified cellular deficiency in *DDHD2*$^{-/-}$ neurons, we, therefore, supplemented the neuronal growth medium with a myristic acid-CoA (Myr-CoA) molecule, aiming at bypassing the cellular need for the lipase activity of DDHD2.

By treating the cultured *DDHD2*$^{-/-}$ neurons with 1 µM Myr-CoA for 48 hours, we observed a full rescue of the mitochondrial respiratory function (Fig. 2B-D, grey lines, and bars) and ATP production (Fig. 2G, grey bar) to the levels comparable to those of C57BL/6J neurons (blue lines and bars). In contrast, non-mitochondrial oxygen consumption was not affected by the supplementation (Fig. 2E), suggesting that providing myristic acid conjugated to CoA might specifically affect mitochondria function. Within the 48-hour rescue, we also did not observe an improvement of the total cellular mitochondrial mass (Fig. 2F), which may require a longer treatment timeframe or supplementation of other sFFAs for a full rescue.

DDHD2$^{-/-}$ neurons have an altered proteome that can be significantly rebalanced by Myr-CoA supplementation.

To study the broad-spectrum cellular changes that could potentially accumulate as a result of the loss of DDHD2 function in neurons, we performed proteomic analysis by label free mass spectrometry in cultured C57BL6/J and *DDHD2*$^{-/-}$ neurons. The effect of Myr-CoA supplementation on the entire proteome was also tested in this experiment. Following mass spectrometry and bioinformatic analysis, we identified 2,511 proteins that were quantified in at least 2 of the 3 replicates for each experimental

group. Replicate reproducibility of the analysis was assessed by principle component (Fig. S2A) and hierarchical clustering (Fig. S2B) analysis, confirming that the proteome identified in each replica consistently clustered according to its respective experimental group (i.e., *DDHD2*$^{-/-}$, *DDHD2*$^{-/-}$ + Myr-CoA treatment, or C57BL6/J).

Further analysis revealed a previously uncharacterized global proteomic shift in *DDHD2*$^{-/-}$ compared to control neurons (Fig. 3A, green dots). Of the 2,511 identified proteins, 965 proteins were significantly (adjusted p-value < 0.05) either up- or down-regulated (Fig. 3A, green dots). Supplementation with 1 µM Myr-CoA for 48 hours significantly reduced this difference (Fig. 3B). Of the 965 proteins that were significantly different in their abundance between the *DDHD2*$^{-/-}$ and control neurons, more than 60% (605 proteins) were no longer significantly different following Myr-CoA treatment (Fig. 3C).

Pathway analysis of proteins associated with pre- and postsynapse, endoplasmic reticulum, Golgi apparatus, as well as mitochondria and transport vesicles, demonstrated that, following Myr-CoA treatment, protein expression levels in each pathway were consistently more similar to the control than to the *DDHD2*$^{-/-}$ group (Fig. 3D-I). In *DDHD2*$^{-/-}$ neurons, large clusters of proteins were either increased (warm colours) or decreased (cold colours) in abundance compared to control neurons. Myr-CoA treatment inverted these protein abundance patterns to levels more comparable to control neurons, resulting in clustering of the C57BL/6J pathways with that of *DDHD2*$^{-/-}$ + Myr-CoA cells. This striking inversion in protein abundance was observed in each analysed pathway (Fig. 3D-I, compare the alignment of *DDHD2*$^{-/-}$ with C57BL/6J and *DDHD2*$^{-/-}$ + Myr-CoA protein distribution). Together, these results demonstrate that a short Myr-CoA treatment was sufficient to significantly rebalance the global *DDHD2*$^{-/-}$ proteome, shifting it towards that of C57BL/6J control cells.

DDHD2 activity is required for efficient synaptic vesicle endocytosis during high frequency stimulation

The retrieval of endocytic membranes at synapses is intricately linked with exocytosis, ensuring the maintenance of appropriate vesicle pools and the preservation of plasma membrane integrity[36,37]. To monitor synaptic vesicle recycling, we utilized the pH-sensitive green fluorescent protein (pHluorin) fused with vesicular glutamate transporter 1 (vGlut1-pH[38]). The construct functions as indicator of synaptic vesicle exo- and endocytosis, and vesicular reacidification: its fluorescence intensity being quenched within the acidic vesicle lumen and subsequently unquenched following synaptic vesicle fusion with the plasma membrane[39]. To explore the role of DDHD2 in synaptic vesicle recycling, hippocampal C57BL6/J control and *DDHD2*$^{-/-}$ neurons, transiently expressing vGlut1-pHluorin, were subjected to high-frequency stimulation, i.e. 50 electric pulses/sec for a duration of 6 sec (50 Hz, 6 s) (Fig. 4A). Before stimulation, the basal fluorescence intensity of the reporter vGlut1-pHluorin was higher in DDHD2 depleted cells compared to control neurons (Figure 4 B, zero time point), indicating that at any given time the extent of vGlut1-pHluorin localized in non-acidic compartments (i.e. plasma membrane and neutral early endosomes) is higher in *DDHD2*$^{-/-}$ neurons compared to control cells. Following stimulation, the fusion of synaptic vesicles to the plasma membrane results in a rapid increase in the vGlut1-pHluorin fluorescence signal that, in our experiments, reached a peak (indicated as 1) in approximately 10 seconds (Fig. 2B). The compensatory retrieval of membranes via endocytosis results in the re-internalization of vGlut1-pHluorin molecules into acidic synaptic vesicles, which corresponds to a gradual decrease in the fluorescence signal of the reporter (Fig. 4B). The rate of fluorescence decline is described by the time constant (t) (i.e. the time required for the fluorescence signal to reach zero if the rate of the decline was linear).

Compared to control neurons (Fig. 4B, blue dots), DDHD2 depleted cells displayed a notable deceleration in the kinetics of vGlut1-pH endocytosis (Fig. 4B, green dots), with a correspondent significant increase in t (Fig. 4C). Concurrent with the delayed endocytosis, EM analysis revealed that the loss of DDHD2 resulted in an enlargement of the presynaptic area under both resting and high K^+

stimulated conditions (Fig. 4D,E). Alongside with presynaptic area, *DDHD2*$^{-/-}$ presynapses exhibited a significantly lower number of synaptic vesicles per presynaptic area (µm2), in both resting and stimulated conditions (Fig. 4F). Notably, the number and the area of endosomes were significantly higher in *DDHD2*$^{-/-}$ presynapses under resting and stimulated conditions (Fig. 4D,G,H). Taken together, our findings revealed that the activity of DDHD2 plays a crucial role in synaptic vesicle recycling, endosome number and size, and maintains presynaptic integrity.

The balance between saturated and unsaturated membrane fatty acid is tightly controlled to maintain normal cellular functions including intracellular trafficking and exocytosis[40]. Indeed, this ratio is a critical factor in determining the molecular 'packing' of lipids which contributes to membrane fluidity[41]. DDHD2 activity-dependent generation of sFFAs could potentially change the lipid composition of the biological membranes, which subsequently would change the membrane fluidity. The ratio of saturated to unsaturated acyl chains in lipids is a critical factor in determining the molecular lipid packing and resulting membrane fluidity. We recently discovered an activity-dependent upregulation of sFFAs in C57BL6J/ neurons, which was absent in *DDHD2*$^{-/-}$ neurons[13]. It could be, therefore, envisioned that the release of sFFAs from biological membranes, such as plasma membrane, could alter membrane fluidity. To investigate this possibility, we performed membrane fluidity measurements using Electron Paramagnetic Resonance (EPR). The results of this analysis demonstrated that compared to resting conditions, following a 5-minute high K^+ stimulation the plasma membrane of control neurons showed an increase in membrane fluidity, as described by the increased membrane order (Fig. S2). The magnitude of this change in *DDHD2*$^{-/-}$ neurons was lower than in control neurons (Fig. S2) indicating that, in addition to regulating neuronal energy levels and synaptic membrane trafficking, DDHD2 activity contributes to membrane biophysics.

Loss of DDHD2 leads to a perturbed balance between synaptic vesicles recycling and activity dependent bulk endocytosis

The recycling of synaptic vesicles is a precisely orchestrated process triggered by various stimuli at synapses[42]. The biogenesis and recycling of synaptic vesicles primarily rely on clathrin-mediated endocytosis (CME) at the presynaptic plasma membrane[42]. After endocytosis, internalized vesicles undergo sorting through a presynaptic endosomal pathway[36,43-45]. To further characterize the function of DDHD2 in synaptic vesicle recycling, we conducted EM analysis of hippocampal neurons derived from both C57BL6/J and *DDHD2*$^{-/-}$ mice. Neurons were stimulated with high K^+ buffer supplemented with 10 mg/ mL of the soluble endocytic cargo horseradish peroxidase (HRP) for 5 minutes, followed by wash with low K^+ buffer and chase for 10 or 30 minutes (Fig. 5A). As expected, we observed a significant decrease in the average endosomal size (HRP-stained endosome sectional area, μm^2) in control neurons following extended chase time from 10 to 30 minutes (Fig. 5A,B). In contrast, the average endosomal size in *DDHD2*$^{-/-}$ neurons increased significantly over time (Fig. 5A,B). In addition, the quantification of percentage of total HRP-stained endocytic structures revealed a significant difference in the distribution of synaptic vesicles and endosomes between control and *DDHD2*$^{-/-}$ neurons (Fig. 5C). The proportion of HRP-stained synaptic vesicles in control neurons was significantly higher than in *DDHD2*$^{-/-}$ neurons following both 10- and 30-min chase times, with majority of the HRP signal being still in endosomes in *DDHD2*$^{-/-}$ neurons.

Next, we performed electric field stimulation involving a train of 300 action potentials delivered at 50Hz for 6 sec in imaging buffer containing HRP (Fig. 5D). In support to our earlier results, the average endosomal area following a 30-minute chase compared to 10 minutes in control neurons decreased significantly, while *DDHD2*$^{-/-}$ neurons exhibited an increase in the average size of HRP-stained endosomes following the prolonged chase time (Fig. 5E). Furthermore, the proportion of HRP-stained synaptic vesicles was significantly higher in control neurons compared with *DDHD2*$^{-/-}$ neurons following both 10- and 30-min chase (Fig. 5F). It is noteworthy, that the 50 Hz (6 second, 300 action

potentials) is a milder stimulus than the 5 min high K^+ buffer stimulation. Accordingly, the high K^+ stimulation induces larger compensatory bulk endosomes than the electric stimulation (Fig. 5B,E). The strong high K^+ stimulation in *DDHD2*$^{-/-}$ neurons blocked the uptake of HRP in synaptic vesicles, indicating a less efficient CME under these conditions, and the activation of compensatory bulk endocytosis.

Supporting these results, EM analysis from repetitive electric field stimulation of both control and *DDHD2*$^{-/-}$ neurons with three sets of 800 action potentials (3x 80 Hz 10 seconds, 800 action potentials, 30 min chase) demonstrated a significant decrease in the number of presynaptic vesicles in *DDHD2*$^{-/-}$ neurons under resting and both mild and stronger stimulatory conditions (Fig. 5G,H). Together, these results indicate that loss DDHD2 perturbs the balance between CME and activity-dependent bulk endocytosis.

Supplementation of Myr-CoA rescues *DDHD2*$^{-/-}$ synaptic vesicle recycling defects, and restores the levels and localization of the clathrin adaptor AP-2

The EM analysis of neurons stimulated with high K^+ revealed an increased size of pre-synaptic area, a decreased number of synaptic vesicles, and an increased number and size of endosomes in stimulated *DDHD2*$^{-/-}$ neurons compared to controls. To test if supplementation of sFFA could rescue these phenotypes, we included Myr-CoA in the neuronal growth medium and used quantitative EM to monitor pre-synaptic area number of synaptic vesicle, and size and number of endosomes following stimulation. This analysis revealed that a 16 h pre-treatment with Myr-CoA was sufficient to decrease the overall presynaptic area in stimulated *DDHD2*$^{-/-}$ neurons, which, although still different, became closer to that of control neurons stimulated under the same condition (Fig. 6A). The number of synaptic vesicles per area was completely restored by the supplementation, becoming non statistically significantly different from that of stimulated control neurons (Fig. 6B). Endosomal area, which was significantly larger in stimulated *DDHD2*$^{-/-}$ neurons became indistinguishable from that of C57BL6/J neurons (Fig. 6C), while the total number of endosomes increased compared to non-supplemented *DDHD2*$^{-/-}$ neurons (Fig. 6D). These results indicated that the administration of Myr-CoA can facilitate the restoration of the balance between activity-dependent bulk endosomes and synaptic vesicle formation and support the notion that large bulk endosomes membranes are a source for synaptic vesicles reformation following high stimulation.

We then investigated further how the loss of DDHD2 affected CME. For this, we performed immunofluorescence staining of tetrameric adaptor protein 2 (AP2) complex, which connects the membrane and endocytic cargo receptors to the structural components of clathrin coat[46,47]. The results demonstrated that loss of DDHD2 is associated with a significant decrease in the endogenous AP2 abundance (Fig. 6A,B) and mislocalization of AP2 to the perinuclear space in the soma. This phenotype was rescued with externally applied Myr-CoA (1 µM, 16 hours), as demonstrated by a significant increase in the abundance of endogenous AP2, and a restoration of the protein localization.

Recent findings suggest that GTP-binding protein ADP-ribosylation factor 6 (Arf6), through the activation of PI_4P_5 kinase, can stimulate the membrane association of AP2[48,49], linking it to both CME, clathrin-independent endocytosis and trafficking of endosomes[48,49]. Plasma membrane localization of Arf6 is strengthened by N-myristoylation, facilitating the recruitment of AP2[50]. Therefore, the observed reduction in sFFAs, inducing myristic acid[13], could be at least in part explained by a possible perturbation of Arf6 N-myristoylation and recruitment of AP2, disturbing CME, which is in line with our EM results (Fig. 4 and 5).

Discussion

We have here demonstrated that the exogenous supplementation of a sFFA, myristic acid, coupled to CoA, can rescue a multitude of defects that we have identified in *DDHD2*$^{-/-}$ neurons. We found that in the absence of DDHD2, the entire proteome is significantly different from that of control neurons, and

that a 48-hour treatment with Myr-CoA significantly, albeit not completely, restores protein homeostasis.

We also found that *DDHD2*$^{-/-}$ neurons have disturbed mitochondrial size, distribution, and functions, and cells have decreased levels of CoA and ATP, even in the presence of glucose. These deficits were also fully restored by Myr-CoA supplementation. The global changes in the protein landscape, along with possible defects in protein lipidation as a result of the observed lower levels of activity-dependent sFFA release in *DDHD2*$^{-/-}$ neurons[13], could explain the defect in mitochondrial function and ATP levels. Alternatively, these results could point to a paradigm change in our basic understanding of neuronal energy production. Historically, neurons have been thought to use glucose as an energy source to fuel the high energy-demanding synaptic-activity. Our data indicate that sFFA might, in fact, be an important source of energy. In conjunction to our study, compelling evidence support the unexpected role of sFFA as an alternative energy source in neurons[51].

Our study links the loss of DDHD2 function to defects in synaptic membrane trafficking, particularly synaptic vesicle recycling and the turnover of bulk endosomes. Our result point to a defect in CME. Although the mechanism behind this defect is currently unknown, recent findings suggest that GTP-binding protein ADP-ribosylation factor 6 (Arf6), through the activation of PI_4P_5 kinase, can stimulate the membrane association of AP2[48,49], linking it to both CME, clathrin-independent endocytosis and trafficking of endosomes[48,49]. Efficient plasma membrane localization and activity of Arf6 require N-myristoylation, which in turn facilitates the recruitment of AP2[50]. Therefore, the observed reduction in sFFAs, inducing myristic acid[13], could lead to a perturbation of Arf6 N-myristoylation and recruitment of AP2, disturbing CME, which is in line with our EM results (Fig. 4 and 5).

Based on our results, we envision that the supplementation of a combination of sFFAs with CoA could provide a successful avenue for therapeutic intervention in spastic paraplegia disorders linked to DDHD2 loss of function. In addition, given the possible role of sFFA as an alternative energy source in the brain, such metabolic supplementation approaches could aid brain function in conditions where glucose utilization becomes less efficient, as it is the case during aging.

Acknowledgements
We would like to acknowledge the facilities, and the scientific and technical assistance, of the Microscopy Australia Facility at the Centre for Microscopy and Microanalysis (CMM) and the Queensland Brain Institute (QBI) Advanced Microscopy Facility, and the facility staff, at The University of Queensland. The authors would also like to acknowledge support from the Queensland Node of Metabolomics and Proteomics Australia for their assistance with metabolomics/proteomics data acquisition. Q-MAP is supported by Bioplatforms Australia, an NCRIS-funded initiative. This work is supported by The University of Queensland Amplify fellowship to MJ, the Academy of Finland (grant number 335527), the European Union's Horizon Europe Research and Innovation Program (grant n umber 101057553), the Helsinki Institute for Life Sciences (HiLIFE), and the Sigrid Juselius Foundation to G.B., The Australian Government Research Training Program (RTP) Scholarship awarded to S.H.S., and N.Y., by The University of Queensland, and WestPac Future Leaders Scholarship to N.Y.

Author Contributions
M.J. conceived and designed the study, and supervised S.H.S., N.Y., S.L., T.B., and R.P. S.H.S performed the mitochondrial respiratory function assays, mass spectrometry together with G.H.T, EPR experiments together with J.H., and electric field stimulation with help from X.L.H.Y. and V.A. N.Y. performed the live cell imaging and quantification of mitochondria. M.J. performed the EM and immunofluorescence analysis and S.L. assisted with EM quantification. A.v.W performed proteomics data analyses. G.B. participated in experimental planning, analysed data. A.G. helped

with data analysis. R.P. and T.B. performed primary tissue culturing and cell culturing, and image analysis. S.H.S, M.J., G.B. wrote the manuscript. All authors participated in proof-reading the manuscript and approved it for publication.

Material and methods

Ethics and mouse strains

All experimental procedures using animals were conducted under the guidelines of the Australian Code of Practice for the Care and Use of Animals for Scientific purposes and were approved by the University of Queensland Animal Ethics Committee (2022/AE000770). DDHD2 knockout (*DDHD2*$^{-/-}$) mice in C57BL6/J background[14] were sourced from the Scripps Research Institute in the United States. Wildtype (C57BL6/J) and *DDHD2*$^{-/-}$ mice were maintained in a 12-hour light/dark cycle (80% intensity), at 18°C − 24°C (30–70% room humidity) and housed in a PC2 facility with ad libitum access to food and water.

Neuronal culturing

Primary hippocampal neurons were obtained from wildtype C57BL6/J and *DDHD2*$^{-/-}$ at embryonic day (E) 16. Isolated hippocampi were prepared and cultured as previously described[52]. Neurons were seeded at 100,000 neurons per 78.54 mm^2 confluency to ensure mature and functional synaptic connections onto poly-L-lysine (Sigma-Aldrich, cat. no. P2636) coated dishes: 1 mg/ mL PLL for glass bottom dishes (CellVis, cat. no. D29-20-1.5-N) and glass coverslips (for live cell imaging and immunofluorescence assays), and 0.1 mg/ mL for plastic dishes (for EM). All experiments were performed at days in vitro (DIV) 20-22.

Ultrastructural electron microscopy analysis and quantification

Electron microscopy (EM) analysis was performed at DIV21-22 on cultured E16 C57BL6/J (± 1 µM IMP-1088 for 16 h) or *DDHD2*$^{-/-}$ hippocampal neurons grown at 100,000 neurons per 78.54 mm^2 confluency to ensure mature and functional synaptic connections on plastic dishes coated with 0.1 mg/mL poly-L-lysine. For ultrastructural analysis of mitochondria and presynapses, neurons were stimulated for 5 minutes in high K^+ buffer (56 mM KCl (Ajax Finechem Pty Limited, cat. no. 1206119), 0.5 mM ascorbic acid (Sigma-Aldrich, cat. no. A5960), 0.1% bovine serum albumin (BSA; Sigma-Aldrich, cat. no. A8022), 15 mM HEPES (Sigma-Aldrich, cat. no. H3375), 5.6 mM D-glucose (AMRESCO, cat. no. 0188), 95 mM NaCl (Sigma-Aldrich, cat. no. S9888), 0.5 mM $MgCl_2$ (Chem-Supply, cat. no. MA029), and 2.2 mM $CaCl_2$ (Sigma-Aldrich, cat. no. C5080) at pH 7.4, 290–310 mOsm) on DIV21-22, and then fixed with 2 % glutaraldehyde (Electron Microscopy Sciences, cat. no. 16210) in 0.1 M sodium cacodylate (Sigma-Aldrich, cat. no. C0250) buffer pH 7.4 for 20 minutes at room temperature, washed three time for 3 minutes with 0.1 M sodium cacodylate buffer, and processed for EM using standard protocols. Control samples were incubated in low K^+ buffer (0.5 mM $MgCl_2$, 2.2 mM $CaCl_2$, 5.6 mM KCl, 145 mM NaCl, 5.6 mM D-glucose, 0.5 mM ascorbic acid, 0.1% (wt/vol) BSA and 15 mM HEPES, pH 7.4, 290–310 mOsm) (i.e. resting condition) for 5 minutes and then fixed as described above. Samples were contrasted with 1 % osmium tetroxide and 2 % uranyl acetate before dehydration and embedded in LX-112 resin using BioWave tissue processing system (Pelco) as previously described [53]. Rescue experiments with 1 µM Myr-CoA for 16 hours were performed on DIV20 by adding the supplement directly into the culture media, and EM samples were prepared as described above on DIV21. Thin sections (80-90 nm) were cut using an ultramicrotome (Leica Biosystems, UC6FCS) and were imaged with a transmission electron microscope (JEOL USA, Inc. model 1101) equipped with cooled charge-coupled device camera (Olympus; Morada CCD Camera). Images were acquired randomly. The quantification of the number synaptic vesicles, the number and size (sectional area, µm^2) endosomes, presynaptic area, mitochondrial size (sectional area, µm^2) in presynapses, axons and somatodendritic compartment, and the number of presynaptic

mitochondria were quantified manually using ImageJ/Fiji[54] (https://imagej.nih.gov/ij/) and Adobe Photoshop (Adobe, 22.4.3 release) Count Tool. Vesicles with sectional area ≤0.002 μm^2 were classified as synaptic vesicles, and those >0.002 μm^2 as endosomes. N = 3 independent neuronal cultures in each condition.

HRP cytochemistry and electron microscopy

For horse radish peroxidase (HRP; Thermo Fisher Scientific, cat. no. 31490) cytochemistry, on DIV21-22, cultured hippocampal C57BL6/J and *DDHD2*$^{-/-}$ neurons were stimulated with high K^+ buffer supplemented with either 10 mg/ mL (high K^+ stimulation assays) or 1 mg/ mL (electric field stimulation assays) horse radish peroxidase for 5 minutes at 37°C in a 5% CO_2 atmosphere, washed with low K^+ buffer (with total volume of 8–10 mL) and chased for either 10 or 30 minutes at 37°C in a 5% CO_2 atmosphere. For electric activity, cultured hippocampal C57BL6/J and *DDHD2*$^{-/-}$ neurons were stimulated by 300 action potential (AP) firing (50 Hz 6 seconds) or 800 action potential (3 x 80 Hz, 10 seconds), and chased for 30 minutes at 37°C in a 5% CO_2 atmosphere. Neurons were then fixed with 2% glutaraldehyde and 2% paraformaldehyde (Electron Microscopy Sciences, cat. no. 15710) in 0.1 M sodium cacodylate (Sigma-Aldrich, cat. no. C0250) buffer, pH 7.4, for 20 minutes at room temperature, washed three times for 3 minutes with 0.1 M sodium cacodylate buffer, and processed for 3,3′-diaminobenzidine tetrahydrochloride (DAB; Sigma-Aldrich, cat. no. D5905) and hydrogen peroxidase (H_2O_2) cytochemistry using standard protocols. Samples were contrasted with 1% osmium tetroxide and 2% uranyl acetate before dehydration and embedded in LX-112 or EPON resin using a BioWave tissue processing system (Pelco) as previously described[55]. An enzymatic reaction of HRP with hydrogen peroxidase and DAB substrates yields an insoluble reaction product that becomes electron dense during osmium tetroxide treatment. Following resin embedding and polymerization, thin sections (80–90 nm) were cut using an ultramicrotome (Leica Biosystems, UC6FCS), and imaged with a transmission electron microscope (JEOL USA, Inc. model 1101) equipped with a cooled charge-coupled device camera (Olympus; Morada CCD camera). Images were acquired when HRP-precipitate was observed in synapses. The quantification of the HRP-positive synaptic vesicles and endosomes was quantified manually using ImageJ/Fiji[54] (https://imagej.nih.gov/ij/) and Adobe Photoshop (Adobe, 22.4.3 release) Count Tool. Vesicles with sectional area ≤0.002 μm^2 were classified as synaptic vesicles, and those >0.002 μm^2 as endosomes. N = 3 independent neuronal cultures in each condition (high K^+), and N=1 independent neuronal cultures in each condition with 3 technical replicates per condition for electric field stimulation.

Live imaging of Mitochondria with Mitotracker

Human small lung carcinoma A549-AT cells were cultured as described previously[56]. The cells were maintained in Dulbecco's Modified Eagle's High Glucose Medium (DMEM, Merck, cat. no. D6546), 1% L-glutamine (Gibco, cat. no. 35050061), 1% non-essential amino acids (NEAA, Gibco, cat. no. 11140050), 10% foetal bovine serum (FBS, Thermo Fisher Scientific, cat. no. 10270-106), 1x penicillin and streptomycin (P/S, Merck, cat. no. P0781) and incubated at 37 °C in 5% CO2 atmosphere. Cells were incubated with 200 nM Mitochondria dye Mitotracker-488 (Millipore, cat. no. SCT136) for 15 minutes at 37 °C in 5% CO_2, then imaged using a Zeiss Plan Apochromat 63x/1.4 NA oil-immersion objective on a confocal/two-photon laser-scanning microscope (LSM 710; Carl Zeiss Pty Ltd, Australia) built around an Axio Observer Z1 body (Carl Zeiss) and equipped with two internal gallium arsenide phosphide (GaAsP) photomultiplier tubes (PMTs) and three normal PMTs for epi-(descanned) detection and two external GaAsP PMTs for non-descanned detection in two-photon imaging, and controlled by Zeiss Zen Black software. The number and size of mitochondria was quantified using ImageJ/Fiji Analyse Particle Tool as described previously[57]. N = 3 independent neuronal cultures in each condition.

Metabolic fluxes in primary neurons

Glycolysis and oxidative phosphorylation are the two major energy-producing pathways in the cell. Most cells possess the ability to switch between these two pathways, thereby adapting to changes in their environment. A valuable and effective experimental method for assessing metabolic fluxes is the Seahorse XFe96 respirometry assay as previously described[58]. The test utilizes the integrated injection ports on XF sensor cartridges to introduce respiratory modulators into the cell well during the assay, unveiling essential mitochondrial function parameters. We monitored the glycolytic flux and mitochondrial respiration in real time by measuring the extracellular acidification rate (ECAR) and oxygen consumption rate (OCR). Briefly, Primary hippocampal from C57 and DDHD2-/- were plated in precoated poly-L-lysine coated (1 mg/ mL) XFe96 multi-well cell plate at density of 25000 cell/well. The key parameters of glycolytic function including basal glycolysis, glycolytic capacity, and glycolytic reserve, were assessed using a Seahorse XF glycolysis assay (Agilent Technologies, Berlin, Germany) according to the manufacturer's instructions. Prior to the assay, XF sensor cartridges were hydrated and calibrated with Seahorse Bioscience calibrant overnight at 37 °C incubator without CO_2. At DIV19-21, neurons viability was checked with microscope and then washed with prewarmed XF assay media DMEM (without phenol red, sodium bicarbonate and sodium pyruvate) for glycolysis or with (DMEM with 10 mM glucoses and 2 mM glutamine and without phenol red, sodium bicarbonate and sodium pyruvate) for Mito stress and the preincubation in assay medium (the same media) for 40 minutes in an incubator at 37 °C without CO2 for 40 minutes. All the glycolysis modulators 20 µL of 60 mM glucose, 20 µL of 7 µM oligomycin, and 20 µL of 1.2 M 2-deoxy-D-glucose (2DG) were sequentially injected in port A, B, and C, while for mitochondrial respiration modulators, 20 µL of 6 µM oligomycin, 20 µL of 14 µM carbonyl cyanide p-trifluoromethoxyphenylhydrazone (FCCP), and 20 µL of 8 µM rotenone/antimycin A (Rot/AA) were serially injected in port A, B, and C. Plate reading and configuration using the Seahorse Analyzer and the Seahorse Wave software will be different from glycol stress to Mito stress.

Fluorometric measurements of Acetyl CoA

Quantifying Acetyl Coenzyme A Level in C57BL6/J and *DDHD2*$^{-/-}$ brain tissues were performed using Acetyl-Coenzyme Assay Kit (Sigma-Aldrich, cat. no. MAK039-1KT). Briefly, 20 mg of brain tissue samples were frozen rapidly in liquid N2 and pulverized. Deproteinize sample by adding 2 µL of 1 M perchloric acid/mg of sample, keeping sample cold. Samples were homogenized and centrifuge d at 10,000 x g for 10 minutes to remove insoluble material. Neutralize the supernatant with 3 M potassium bicarbonate solution adding in aliquots of 1 µL/10 µL of supernatant while vertexing until bubble evolution ceases (2–5 aliquots) and then cool on ice for 5 minutes and finally Spin 2 minutes to pellet potassium bicarbonate. 10 µL of the samples was added to 40 µL of acetyl-CoA assay buffer (include in the kit). 50 µL of the Reaction Mix to each well and mixed well using a horizontal shaker and incubate the reaction for 10 minutes at 37 ºC in the dark to protect from light. Measure fluorescence intensity (λex = 535/ λem = 587 nm). Quantifying the Acetyl CoA was done against standard curve according to manufacturer's instructions.

Proteomics analysis using high resolution Orbitrap mass spectrometry

The LC/MS/MS identification and quantification of the digested peptides from primary hippocampal neurons from C57BL6/J, *DDHD2*$^{-/-}$ and *DDHD2*$^{-/-}$ treated with 1 µM Myristoyl coenzyme A lithium salt (Myr-CoA, Sigma-Aldrich, cat. no. M4414) were performed using a S-Trap™ (Protifi, NY) Micro Spin Column Digestion protocol. Briefly, samples were solubilised by adding 50 µL of S-Trap lysis buffer (10% sodium dodecyl sulphate (SDS) in 100 mM Tris, pH 8.0) to 50 µL of sample, before reducing by adding 20 mM of dithiothreitol (DTT) and heating at 70°C for 60 minutes. Cysteine residues were alkylated to prevent disulphide bond reformation using 40 mM iodoacetamide for 30 minutes at room temperature in the dark. 2.5 µL of 12% phosphoric acid was added, followed by 165 µL of S-Trap binding buffer (90% methanol in 100 mM Tris) to the acidified lysate. The sample mix was then centrifuged through the S-Trap column at 4,000 x g for 1 minute followed by three washes

with 150 µL S-Trap binding buffer, with 4,000 x g centrifugation between each wash. Peptide digestion was initiated by adding 25 µL of 50 mM ammonium bicarbonate buffer (pH 8) containing 2 µg trypsin (Sequencing Grade Modified Trypsin, Promega, cat. no. V5117) directly on top of the column and incubating overnight at 37 °C in anoven. Peptides were eluted by three successive aliquots of 40 µL of 5%, 50%, and 75% acetonitrile in 0.1% formic acid, respectively. Eluted peptides were dried down using a vacuum concentrator (Concentrator Plus, Eppendorf).

The samples were redissolved in 20 µl of 5%ACN (aq) and 2 µl were injected to a trap column (Thermo 22mmx300µm, 5µm, C18) at a flow rate of 10µL/min. Following 3 min wash the trap column was switched in-line with a resolving column (Water nanoEase 100mmx150µm, 1.8µm, 100Å). The samples were eluted by a gradient was held constant at 8% for 4 minutes, then was increased linearly to 24% at 47 minutes, to 40% at 53 minutes and to 95% at 57 minutes. The gradient held constant for 1 minute, before returning to start condition at 8% over 1 minute. Mass spectrometry using LC-MS/MS was performed using a Ultimate UHPLC system coupled to an Exploris 480 mass spectrometer with a FAIMS Pro interface (Thermo Fisher Scientific) The FAIMS compensation voltages were -45 V and -65 V. The electrospray voltage was 2.2 kV in positive-ion mode, and the ion transfer tube temperature was 295°C. Full MS scans were acquired in the Orbitrap mass analyser over the range of m/z 340-1110 with a mass resolution of 120,000. The automatic gain control (AGC) target value was set at 'Standard', and the maximum accumulation time was 'Auto' for the MS. The MS/MS ions were measured in 6 windows from mass 350-470, in 18 windows from mass 465-645 and 5 windows from mass 640-1100 with an overlap of 1 m/z and quadrupole isolation mode. Analysis of data were performed using Spectronaut against a reference proteome with a Q-value cut-off of 0.05.

Additional processing and statistical analysis of label-free mass-spectrometry

The standard, non-normalised output of Spectronaut (BGS Factory Report text file) was imported into R version 4.05 for further processing using a modified method described previously[59]. For proteins that mapped to multiple annotations, the 'best annotation' method previously described was used[59]. Each sample group was permitted to have up to one missing value (that is, an intensity not reported one or three individual replicates). Protein intensities of the parent group protein 'PG.ProteinGroups' were then log2 transformed and globally normalised using the quantile normalisation method[60]. Missing values were assumed to be missing at random and imputed using the knn nearest neighbour averaging method[61]. Following, unwanted sources of technical variation were removed by surrogate variable analysis[62]. Sample clustering was confirmed using unsupervised principal component analysis and hierarchical clustering. Principle Component Analysis of the first two principal components using singular value decomposition, as implemented in pcaMethods version 1.82.0 and hierarchical clustering using 'ward' method for clustering distance 'euclidean'. For hierarchical clustering, probabilities of clustering were determining using 100 bootstrap replications, as implemented in pvcluster version 2.2-0, and probabilities of the branch positions shown in the plot, together with the probabilities of clusters (red boxes). For differential protein abundance, generalised linear modelling with Bayes shrinkage as implemented in limma version 3.46.0 was performed and proteins were considered differentially abundant at a corrected p-value of 0.05 unless specified otherwise (adjusted for false discovery rate using the Benjamini and Hochberg method)[63].

Gene Set Enrichment Analyses

Heatmaps for proteins belonging to a gene set (gene ontology term) were independently generated by extracting all Gene Symbols from 'org.Mm.eg.db' version 3.1.2 that matched a specific GO term of interest. This was then filtered by proteins that were differentially abundant between DDHD2KO myristic treated (nonstim) versus DDHD2KO (nonstim) (or comparison of interest). The z-score of the protein intensities across all samples (row-wise) was then calculated across samples and plot as a heatmap using the pheatmap version 1.0.12. Clustering distance was 'euclidean' and clustering method 'complete' linkage. Targeted pathways selected included: 'Mitochondria (GO:0005739)', 'Presynapse

(GO:0098793)', 'the endoplasmic reticulum (GO:0005783)', 'endoplasmic reticulum–Golgi intermediate compartment (GO:0005793)', 'ER to Golgi transport vesicle (GO:0030134)', 'Golgi apparatus (GO:0005794)', 'secretory granule (GO:0030141)', 'transport vesicle (GO:0030133)', and 'ribosome (GO:0005840)'.

Fluorescence imaging of vGlut1-pHluorin trafficking

Live hippocampal neurons expressing vGlut1-pHluorin were mounted in an imaging chamber with field stimulation electrodes (RC-21BRFS; Warner Instruments, Hamden, CT) and continuously perfused with imaging buffer (119 mM NaCl, 2.5 mM KCl, 2 mM $CaCl_2$, 2 mM $MgCl_2$, 25 mM HEPES, 30 mM D-glucose, pH 7.4) supplemented with 10 µM NBQX (Abcam, cat. no. ab120046) and 50 µM DL-APV (Abcam, cat. no. ab120271). All experiments were performed at 35°C. The imaging solution was kept constant at 35°C using an inline solution heater (SH-27B; Warner Instruments). Neurons expressing vGlut1-pHluorin were challenged with a train of 300 action potentials delivered at 50Hz, 6 seconds (100 mA and 1ms pulse width) and imaged at 0.5 Hz (2 × 2 binning) through a 40X (1.4 NA) oil objective using an inverted Zeiss Axio Observer Z1 epifluorescence microscope equipped with an Andor Luca R EMCCD camera. pHluorin fluorescence was imaged at 488 nm excitation and collected through a 500-550 nm emission filter. At the end of the imaging session, neurons were perfused with an alkaline imaging buffer (50 mM NH_4Cl substituted for 50 mM NaCl) to reveal total pHluorin expression. Equal-sized regions of interest were placed over nerve terminals to measure the pHluorin fluorescence elicited by stimulation over time using the Time Series Analyzer plugin in FIJI software (NIH). Activity-dependent changes in fluorescence (ΔF/F0) were normalized to the respective peak heights from the train of stimuli (to calculate the rate of endocytosis) or to the total amount of fluorescence present after alkaline treatment (to calculate the exocytosis amplitude). The endocytosis time constant (τ value) was calculated by fitting the decay phase for each trace to a single exponential function [38]. N = 3 independent neuronal cultures in each condition.

Electron paramagnetic resonance measurements (EPR)

To assess membrane fluidity, nitroxyl radicals SLFA probes will be used; Spin-labeled stearic acids 2-(3-carboxypropyl)-4,4-dimethyl-2-tridecyl-3-oxazolidinyloxy (5-doxyl-stearic acid, 5-DSA, cat. no. 253618) and 2-(14-carboxytetradecyl)-2-ethyl-4,4-di methyl-3-oxazolidinyloxy (16-doxyl-stearic acid, 16-DSA, cat. no. 253596) were purchased from Sigma-Aldrich. 5-DSA (spin probe containing the nitroxide group attached on C5 that is located on the opposite terminal relative to the charged carboxyl fatty acid terminus) to determine the local fluidity near the protein/aqueous interface or 16-DSA (spin probe containing the nitroxide group attached on C16 that is located on the opposite terminal relative to the charged carboxyl fatty acid terminus) to assess the fluidity near the hydrophobic protein cores. C57BL6/J and *DDHD2*$^{-/-}$ neurons, and neurosecretory PC12 cells (cultured as previously described[64]) were labelled 0.02 M ethanolic solutions of 5-DSA or 16-DSA and loaded into the capillary tubes and measure the electron paramagnetic resonance (EPR) spectra at 37°C using a Bruker E540 Benchtop Magnettech MiniScope MS5000 spectrometer (now Bruker Biospin, Berlin) equipped with biotemperature control and computerized data acquisition and analysis capabilities. Typical instrumental parameters for these measurements will be microwave frequency 9.47 86 GHz, microwave power 5.024 mW (16 dB attenuation of 200 mW source)0 mW, modulation frequency 100 kHz, modulation amplitude 0.12 mT (16-DSA) or 0.3 mT (5-DSA). Resonances occur in the approximate, and magnetic field range 332346–342 356 mT. The number of scans varied depending upon the required signal-to-noise ratio; each scan was 60 seconds, and the measurement time was typically 5 to 10 minutes Each spectrum will be the average of 5-10 scans with scan time of 60 seconds. Analysis of biophysical EPR parameters fluidity measurement will be carried out as previously reported [78].

Immunofluorescence

Rescue experiments with 1 µM Myr-CoA for 16 hours were performed on DIV20 on cultured *DDHD2*$^{-/-}$ neurons by adding the supplement directly into the culture media. C56BL6/J and *DDHD2*$^{-/-}$ neurons were fixed on DUV21 in 4% paraformaldehyde in PBS for 30 minutes at room temperature. They were then washed in PBS and permeabilized with 0.1% Triton x100 (Sigma-Aldrich-Merck, cat. no. X100-100ML) for 4 minutes. After permeabilization and blocking with 1% BSA in PBS for 30 minutes at room temperature, neurons were stained for endogenous AP2 with Anti-AP-2 complex subunit alpha-1 goat polyclonal primary antibody (1:1000, Abcam, cat. no. ab218624) that was diluted in blocking solution (1% BSA in PBS) over night at 4 ºC. Next day, samples were immunostained using donkey anti-goat Alexa Fluor® 647 (1:2000, Thermo Fisher Scientific, cat. no. A21447) secondary antibody diluted in blocking solution (1% BSA in PBS) for 45 minutes at room temperature. Neurons were stained with DAPI (Sigma-Aldrich, cat. no. D9542) and Phalloidin Atto 647N (Sigma-Aldrich, cat. no. 65906) according to manufacturer's protocols. Finally, neurons were washed and mounted in ProLong Gold Antifade Mountant (Thermo Fisher Scientific, cat. no. P36934). Confocal images of fixed samples were acquired with a spinning-disk confocal system consisting of an Axio Observer Z1 equipped with a CSU-W1 spinning-disk head, ORCA-Flash4.0 v2 sCMOS camera, 63x 1.3 NA C-Apo objective. Image acquisition was performed using SlideBook 6.0. Sections of each slide were acquired using a Z-stack with a step of 100 nm. The exposure time for each channel was kept constant across all imaging sessions. Images were deconvolved on Huygens deconvolution software 21.10 (Scientific Volume Imaging). For the quantification of AP2 levels in C57BL6/J and *DDHD2*$^{-/-}$ neurons, fluorescence images acquired by confocal microscopy using identical microscope settings where first Z-projected using the Image-J software (Fiji version). The quantification of AP2 fluorescence was then performed using the Cell profiler 4 software (www.cellprofiler.org). First the nuclei (Primary Object) of the neurons were selected using the "Identify Primary Object" tool with the Otzu algorithm inbuilt in the software. Apoptotic nuclei, which were significantly smaller than healthy nuclei, were excluded from the analysis by automatic size exclusion. The perimeter of the cell cytoplasm was then automatically detected using the AP2 fluorescence channel by using the "Identify secondary object" tool of the software with the Otzu algorithm and a very sensitive threshold of segmentation so that the whole cell contour was accurately outlines even in cells with very low AP2 levels. From this 'secondary object', the nuclear area was excluded using the "Identify Tertiary Object" tool of the software. The resulting area of the 'tertiary object' was used to quantify the levels of AP2 per cell. Visual inspection was performed for each image to make sure the segmentation of the cell cytoplasm was accurate. Obtained values where then background subtracted and normalized to the intensity of fluorescence of the respective nuclei stained with the nuclear dye Hoechst.

References:

1 Mackay-Sim, A. Hereditary Spastic Paraplegia: From Genes, Cells and Networks to Novel Pathways for Drug Discovery. *Brain Sci* **11**, doi:10.3390/brainsci11030403 (2021).

2 Schüle, R. & Schöls, L. in *Seminars in neurology.* 484-493 (© Thieme Medical Publishers).

3 Blackstone, C. Cellular pathways of hereditary spastic paraplegia. *Annual review of neuroscience* **35**, 25-47 (2012).

4 Giudice, T. L., Lombardi, F., Santorelli, F. M., Kawarai, T. & Orlacchio, A. Hereditary spastic paraplegia: clinical-genetic characteristics and evolving molecular mechanisms. *Experimental neurology* **261**, 518-539 (2014).

5 Nicita, F. *et al.* Defining the clinical-genetic and neuroradiological features in SPG54: description of eight additional cases and nine novel DDHD2 variants. *Journal of Neurology* **266**, 2657-2664 (2019).

6 Blackstone, C. Hereditary spastic paraplegia. *Handbook of clinical neurology* **148**, 633-652 (2018).

7 Salinas, S., Proukakis, C., Crosby, A. & Warner, T. T. Hereditary spastic paraplegia: clinical features and pathogenetic mechanisms. *The Lancet Neurology* **7**, 1127-1138 (2008).

8 Fink, J. K. Hereditary spastic paraplegia. *Current neurology and neuroscience reports* **6**, 65-76 (2006).
9 Murala, S., Nagarajan, E. & Bollu, P. C. Hereditary spastic paraplegia. *Neurological Sciences* **42**, 883-894 (2021).
10 Schuurs-Hoeijmakers, J. H. *et al.* Mutations in DDHD2, encoding an intracellular phospholipase A1, cause a recessive form of complex hereditary spastic paraplegia. *The American Journal of Human Genetics* **91**, 1073-1081 (2012).
11 Joensuu, M., Wallis, T. P., Saber, S. H. & Meunier, F. A. Phospholipases in neuronal function: A role in learning and memory? *Journal of neurochemistry* **153**, 300-333 (2020).
12 Wallis, T. P. *et al.* Saturated free fatty acids and association with memory formation. *Nat Commun* **12**, 3443, doi:10.1038/s41467-021-23840-3 (2021).
13 Akefe, I. O. *et al.* DDHD2 interacts with STXBP1 to mediate long-term memory via the generation of myristic acid. *bioRxiv*, 2023.2005. 2011.540316 (2023).
14 Inloes, J. M. *et al.* The hereditary spastic paraplegia-related enzyme DDHD2 is a principal brain triglyceride lipase. *Proceedings of the National Academy of Sciences* **111**, 14924-14929 (2014).
15 Inloes, J. M. *et al.* Functional Contribution of the Spastic Paraplegia-Related Triglyceride Hydrolase DDHD2 to the Formation and Content of Lipid Droplets. *Biochemistry* **57**, 827-838, doi:10.1021/acs.biochem.7b01028 (2018).
16 Inoue, H. *et al.* Roles of SAM and DDHD domains in mammalian intracellular phospholipase A1 KIAA0725p. *Biochimica et Biophysica Acta (BBA)-Molecular Cell Research* **1823**, 930-939 (2012).
17 Sato, S.-i., Inoue, H., Kogure, T., Tagaya, M. & Tani, K. Golgi-localized KIAA0725p regulates membrane trafficking from the Golgi apparatus to the plasma membrane in mammalian cells. *FEBS letters* **584**, 4389-4395 (2010).
18 Maruyama, T. *et al.* Loss of DDHD2, whose mutation causes spastic paraplegia, promotes reactive oxygen species generation and apoptosis. *Cell death & disease* **9**, 797 (2018).
19 Gonzalez, M. *et al.* Mutations in phospholipase DDHD2 cause autosomal recessive hereditary spastic paraplegia (SPG54). *European journal of human genetics* **21**, 1214-1218 (2013).
20 Pietrocola, F., Galluzzi, L., Bravo-San Pedro, J. M., Madeo, F. & Kroemer, G. Acetyl coenzyme A: a central metabolite and second messenger. *Cell Metab* **21**, 805-821, doi:10.1016/j.cmet.2015.05.014 (2015).
21 Lezi, E. & Swerdlow, R. H. Mitochondria in neurodegeneration. *Advances in mitochondrial medicine*, 269-286 (2012).
22 Tesson, C. *et al.* Alteration of fatty-acid-metabolizing enzymes affects mitochondrial form and function in hereditary spastic paraplegia. *The American Journal of Human Genetics* **91**, 1051-1064 (2012).
23 Maruyama, T. *et al.* Loss of DDHD2, whose mutation causes spastic paraplegia, promotes reactive oxygen species generation and apoptosis. *Cell death & disease* **9**, 1-15 (2018).
24 Baba, T. *et al.* Phosphatidic acid (PA)-preferring phospholipase A1 regulates mitochondrial dynamics. *Journal of Biological Chemistry* **289**, 11497-11511 (2014).
25 Inloes, J. M., Jing, H. & Cravatt, B. F. The Spastic Paraplegia-Associated Phospholipase DDHD1 Is a Primary Brain Phosphatidylinositol Lipase. *Biochemistry* **57**, 5759-5767, doi:10.1021/acs.biochem.8b00810 (2018).
26 Kameoka, S., Adachi, Y., Okamoto, K., Iijima, M. & Sesaki, H. Phosphatidic acid and cardiolipin coordinate mitochondrial dynamics. *Trends in cell biology* **28**, 67-76 (2018).
27 Mousnier, A. *et al.* Fragment-derived inhibitors of human N-myristoyltransferase block capsid assembly and replication of the common cold virus. *Nat Chem* **10**, 599-606, doi:10.1038/s41557-018-0039-2 (2018).
28 Demetriadou, A. *et al.* Mouse Stbd1 is N-myristoylated and affects ER-mitochondria association and mitochondrial morphology. *J Cell Sci* **130**, 903-915, doi:10.1242/jcs.195263 (2017).
29 Fhu, C. W. & Ali, A. Protein Lipidation by Palmitoylation and Myristoylation in Cancer. *Front Cell Dev Biol* **9**, 673647, doi:10.3389/fcell.2021.673647 (2021).

30 Bollu, L. R. *et al.* Involvement of de novo synthesized palmitate and mitochondrial EGFR in EGF induced mitochondrial fusion of cancer cells. *Cell Cycle* **13**, 2415-2430, doi:10.4161/cc.29338 (2014).
31 Monzio Compagnoni, G. *et al.* The role of mitochondria in neurodegenerative diseases: the lesson from Alzheimer's disease and Parkinson's disease. *Molecular neurobiology* **57**, 2959-2980 (2020).
32 Fukui, H. & Moraes, C. T. Mechanisms of formation and accumulation of mitochondrial DNA deletions in aging neurons. *Hum Mol Genet* **18**, 1028-1036, doi:10.1093/hmg/ddn437 (2009).
33 Swerdlow, R. H., Burns, J. M. & Khan, S. M. The Alzheimer's disease mitochondrial cascade hypothesis. *J Alzheimers Dis* **20 Suppl 2**, S265-279, doi:10.3233/JAD-2010-100339 (2010).
34 Baloyannis, S. J. Mitochondrial alterations in Alzheimer's disease. *Journal of Alzheimer's disease* **9**, 119-126 (2006).
35 Zhang, L. *et al.* Altered brain energetics induces mitochondrial fission arrest in Alzheimer's Disease. *Scientific reports* **6**, 18725 (2016).
36 Heuser, J. & Reese, T. Evidence for recycling of synaptic vesicle membrane during transmitter release at the frog neuromuscular junction. *The Journal of cell biology* **57**, 315-344 (1973).
37 Haucke, V., Neher, E. & Sigrist, S. J. Protein scaffolds in the coupling of synaptic exocytosis and endocytosis. *Nature Reviews Neuroscience* **12**, 127-138 (2011).
38 Yong, X. L. H., Cousin, M. A. & Anggono, V. PICK1 controls activity-dependent synaptic vesicle cargo retrieval. *Cell Reports* **33** (2020).
39 Wang, L. *et al.* α-synuclein multimers cluster synaptic vesicles and attenuate recycling. *Current Biology* **24**, 2319-2326 (2014).
40 Ali, O. & Szabó, A. Review of Eukaryote Cellular Membrane Lipid Composition, with Special Attention to the Fatty Acids. *International Journal of Molecular Sciences* **24**, 15693 (2023).
41 Baccouch, R. *et al.* The impact of lipid polyunsaturation on the physical and mechanical properties of lipid membranes. *Biochimica et Biophysica Acta (BBA)-Biomembranes* **1865**, 184084 (2023).
42 Morgan, J. R., Comstra, H. S., Cohen, M. & Faundez, V. Presynaptic membrane retrieval and endosome biology: defining molecularly heterogeneous synaptic vesicles. *Cold Spring Harbor Perspectives in Biology* **5**, a016915 (2013).
43 Milosevic, I. Revisiting the role of clathrin-mediated endoytosis in synaptic vesicle recycling. *Frontiers in Cellular Neuroscience* **12**, 27 (2018).
44 Murthy, V. N. & Camilli, P. D. Cell biology of the presynaptic terminal. *Annual review of neuroscience* **26**, 701-728 (2003).
45 Partlow, E. A., Cannon, K. S., Hollopeter, G. & Baker, R. W. Structural basis of an endocytic checkpoint that primes the AP2 clathrin adaptor for cargo internalization. *Nature structural & molecular biology* **29**, 339-347 (2022).
46 Zaremba, S. & Keen, J. H. Assembly polypeptides from coated vesicles mediate reassembly of unique clathrin coats. *The Journal of cell biology* **97**, 1339-1347 (1983).
47 Pearse, B. & Robinson, M. Purification and properties of 100-kd proteins from coated vesicles and their reconstitution with clathrin. *The EMBO journal* **3**, 1951-1957 (1984).
48 Krauss, M. *et al.* ARF6 stimulates clathrin/AP-2 recruitment to synaptic membranes by activating phosphatidylinositol phosphate kinase type Iγ. *The Journal of cell biology* **162**, 113-124 (2003).
49 Franco, M. *et al.* EFA6, a sec7 domain-containing exchange factor for ARF6, coordinates membrane recycling and actin cytoskeleton organization. *The EMBO journal* **18**, 1480-1491 (1999).
50 Padovani, D., Zeghouf, M., Traverso, J. A., Giglione, C. & Cherfils, J. High yield production of myristoylated Arf6 small GTPase by recombinant N-myristoyl transferase. *Small GTPases* **4**, 3-8 (2013).
51 Kumar, M. *et al.* DDHD2 is necessary for activity-driven fatty acid fueling of nerve terminal function. *bioRxiv*, 2023.2012.2018.572201, doi:10.1101/2023.12.18.572201 (2023).
52 Joensuu, M. *et al.* Visualizing endocytic recycling and trafficking in live neurons by subdiffractional tracking of internalized molecules. *Nature protocols* **12**, 2590-2622 (2017).
53 Rigoni, M. *et al.* Equivalent effects of snake PLA2 neurotoxins and lysophospholipid-fatty acid mixtures. *Science (New York, N.Y.)* **310**, 1678-1680, doi:10.1126/science.1120640 (2005).

54 Schindelin, J. *et al.* Fiji: an open-source platform for biological-image analysis. *Nat Methods* **9**, 676-682, doi:10.1038/nmeth.2019 (2012).

55 Joensuu, M. *et al.* Presynaptic targeting of botulinum neurotoxin type A requires a tripartite PSG-Syt1-SV2 plasma membrane nanocluster for synaptic vesicle entry. *EMBO J* **42**, e112095, doi:10.15252/embj.2022112095 (2023).

56 Saber, S. H. *et al.* The infectivity of SARS-CoV-2 progeny virions requires the activity of host cell N-myristoyltransferases and it is severely compromised by their inhibition. *bioRxiv*, 2023.2003.2003.530798, doi:10.1101/2023.03.03.530798 (2023).

57 Lopez-Cano, M., Fernandez-Duenas, V. & Ciruela, F. Proximity Ligation Assay Image Analysis Protocol: Addressing Receptor-Receptor Interactions. *Methods Mol Biol* **2040**, 41-50, doi:10.1007/978-1-4939-9686-5_3 (2019).

58 Marinangeli, C., Kluza, J., Marchetti, P., Buee, L. & Vingtdeux, V. Study of AMPK-regulated metabolic fluxes in neurons using the seahorse XFe analyzer. *AMPK: Methods and Protocols*, 289-305 (2018).

59 Engholm-Keller, K. *et al.* The temporal profile of activity-dependent presynaptic phospho-signalling reveals long-lasting patterns of poststimulus regulation. *PLoS biology* **17**, e3000170 (2019).

60 Bolstad, B. M., Irizarry, R. A., Åstrand, M. & Speed, T. P. A comparison of normalization methods for high density oligonucleotide array data based on variance and bias. *Bioinformatics* **19**, 185-193 (2003).

61 Troyanskaya, O. *et al.* Missing value estimation methods for DNA microarrays. *Bioinformatics* **17**, 520-525 (2001).

62 Leek, J. T., Johnson, W. E., Parker, H. S., Jaffe, A. E. & Storey, J. D. The sva package for removing batch effects and other unwanted variation in high-throughput experiments. *Bioinformatics* **28**, 882-883 (2012).

63 Ritchie, M. E. *et al.* limma powers differential expression analyses for RNA-sequencing and microarray studies. *Nucleic acids research* **43**, e47-e47 (2015).

64 Kasula, R. *et al.* The Munc18-1 domain 3a hinge-loop controls syntaxin-1A nanodomain assembly and engagement with the SNARE complex during secretory vesicle priming. *J Cell Biol* **214**, 847-858, doi:10.1083/jcb.201508118 (2016).

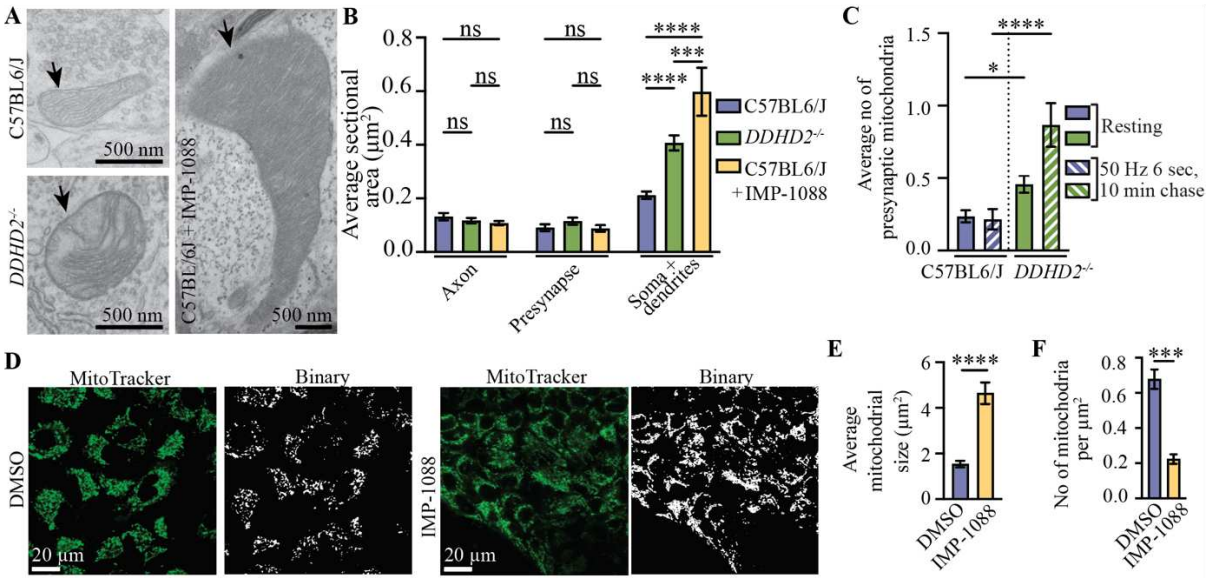

Figure 1. Loss of DDHD2 leads to mitochondrial enlargement in the soma and accumulation in presynapses. (A) Representative electron microscopy (EM) images of mitochondria (arrows) in cultured E16 C57BL6/J and *DDHD2*$^{-/-}$ hippocampal neurons at DIV21-22, as well as C57BL6/J hippocampal neurons treated with 1 µM IMP-1088 for 16 h. (B) Quantification of average sectional area (µm^2) of mitochondria from EM images (obtained from 80-90 nm thin sections) in indicated regions of interest. Results shown as average ± sem, 2way ANOVA with Tukey's multiple comparisons test, non-significant (ns), ***p<0.001, ****p<0.0001, N = 3 independent experiments in each condition. (C) Quantification of number of mitochondria in cultured E16 C57BL6/J and *DDHD2*$^{-/-}$ hippocampal neuron (DIV21-22) presynapses from EM images (obtained from 80-90 nm thin sections) in resting (non-stimulated) condition and following a stimulation with a train of 300 action potentials (50 Hz, 6 s) and 10 chase at 37°C cell culture incubator. Results shown as average ± sem, Kruskal-Wallis multiple comparisons test, *p<0.05, ****p<0.0001, N = 3 independent experiments in each condition. (D) Representative confocal images of vehicle (DMSO) or IMP-1088 (1 µM for 48 h) treated A549 cells and imaged using MitoTracker dye. Basolateral optical sections were transformed into binary images, and the (E) size (µm^2) and (F) number of mitochondria per cell area µm^2 was quantified using Fiji/ ImageJ spot detection function. Results shown as average ± sem, student's t test, ***p<0.001, ****p<0.0001, N = 2 independent experiments in both conditions.

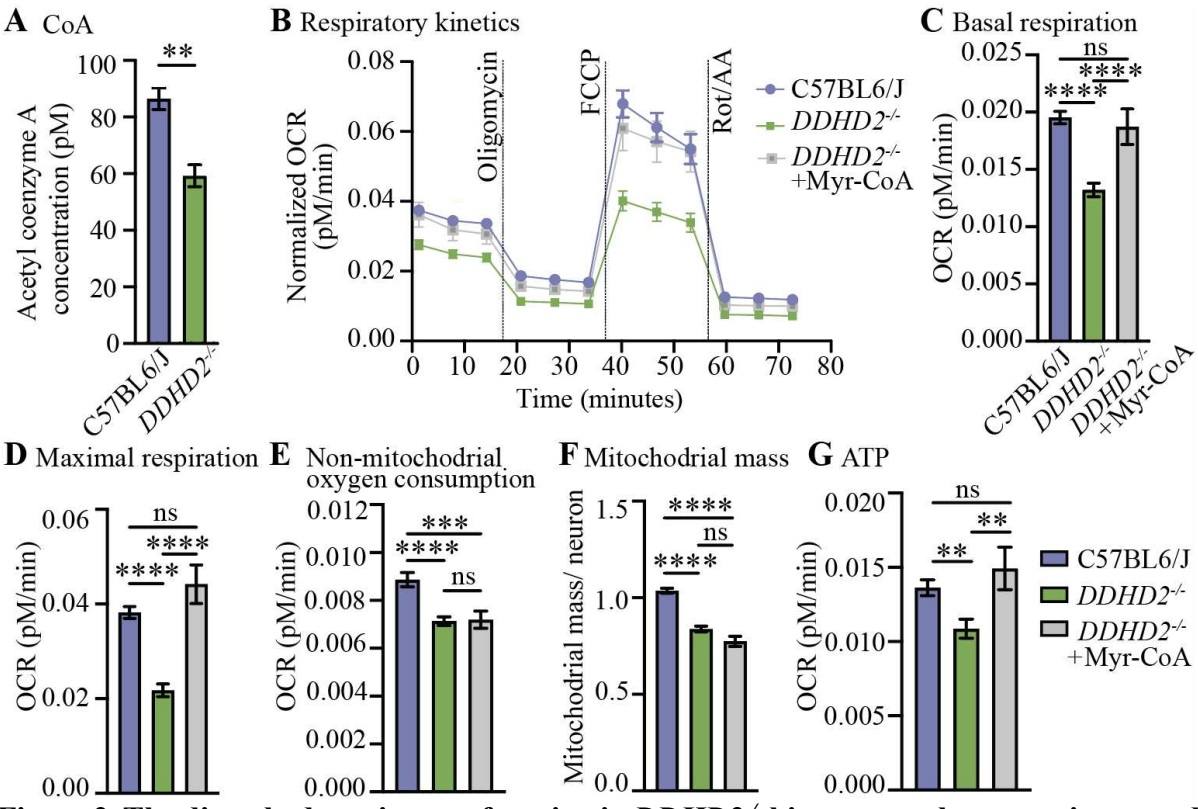

Figure 2. The disturbed respiratory function in *DDHD2*$^{-/-}$ hippocampal neurons is rescued with myristoyl-coenzyme A. (A) Quantification of Acetyl-Coenzyme A (CoA) levels in C57BL6/J and *DDHD2*$^{-/-}$ brain lysates using a fluorometric assay. Results shown as average ± sem, student's t test, **p<0.01, N = 2 independent experiments in both conditions. (B) Seahorse XF measurement of oxygen consumption rate (OCR) in cultured E16 neurons from C57BL6/J, *DDHD2*$^{-/-}$ and *DDHD2*$^{-/-}$ treated with 1 µM Myr-CoA for 48 h. Injection of oligomycin (an ATP synthase inhibitor), phenylhydrazone (FCCP; an uncoupling agent that collapses the proton gradient and disrupts the mitochondrial membrane potential) and Rot (Rotenone, mitochondrial complex I inhibitor) AA (Antimycin A, mitochondrial a complex III inhibitor) are indicated. Results shown as average ± sem, N = 3 independent experiments in each condition. Quantification of OCR (C) basal respiration, (D) maximal respiration, (E) non-mitochondrial oxygen consumption, (F) mitochondrial mass and (G) ATP production in indicated conditions. Results shown as average ± sem, Kruskal-Wallis multiple comparisons test, non-significant (ns), **p<0.01, ****p<0.0001, N = 3 independent experiments in each condition.

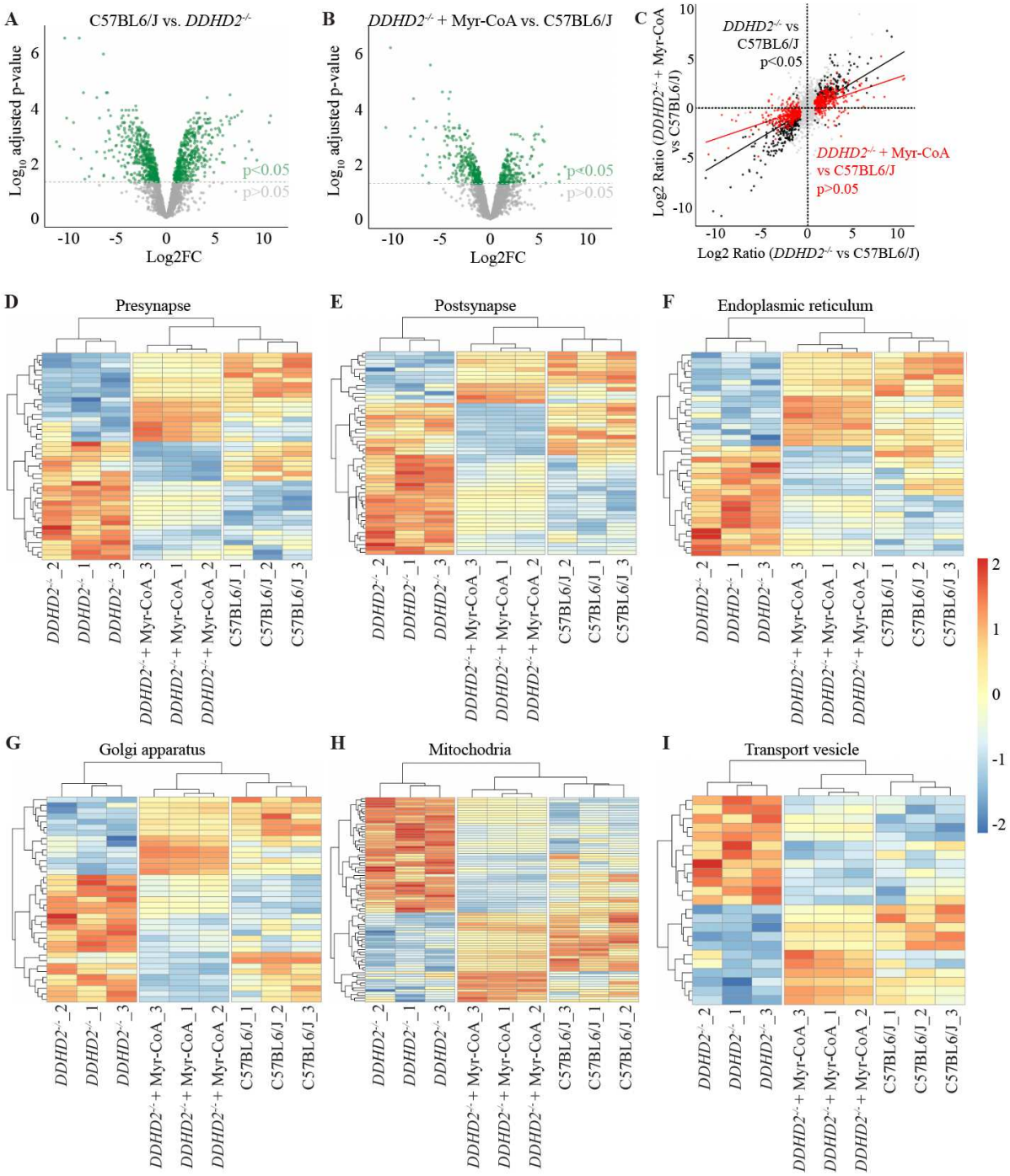

Figure 3. Alterations in the *DDHD2*$^{-/-}$ hippocampal neuron proteome can be partially rescued with Myr-CoA. The proteomes of cultured E16 neurons from C57BL6/J, *DDHD2*$^{-/-}$ and *DDHD2*$^{-/-}$ treated with 1 µM Myr-CoA for 48 h, were analysed by mass spectrometry. (A--B) Differentially abundant proteins are visualised as a volcano plot, representing the log2 FC (or ratio) of the XX vs. YY, on the x-axis and the -log10 transformed adjusted p-value on the Y-axis (increased significance becomes a higher value). The threshold of an adjusted p-value of 0.05 is represented as a dotted grey line. (C) Myr treatment shifts proteome towards Wild type. Protein abundance of *DDHD2*$^{-/-}$ versus C57BL6/J on the x-axis and *DDHD2*$^{-/-}$ with Myr-CoA treatment versus C57BL6/J on the y-axis. Black dots indicate proteins that significantly differentially abundant in the *DDHD2*$^{-/-}$ vs C57BL6/J (965 proteins). Red Dots are proteins that were also significantly differentially abundant in the *DDHD2*$^{-/-}$ vs C57BL6/J but are not longer significantly differentially abundant after myristic acid (605 proteins). Grey points

indicate proteins that not statistically differentially abundant in the *DDHD2*$^{-/-}$ vs C57BL6/J comparison. The black and red lines correspond to linear model fits to these sets of proteins, highlighting the *DDHD2*$^{-/-}$ proteome that is shifting towards C57BL/6J. N=3 independent experiments in each condition. (D-I) Protein abundance heatmap for indicated pathways in neurons from C57BL6/J, *DDHD2*$^{-/-}$ and *DDHD2*$^{-/-}$ treated with 1 µM Myr-CoA for 48 h. Each row represents an individual protein. Cells are coloured by the z-score, which is calculated for each row. Samples (Columns) and proteins (rows) are clustered 'euclidean' method with 'complete' linkage.

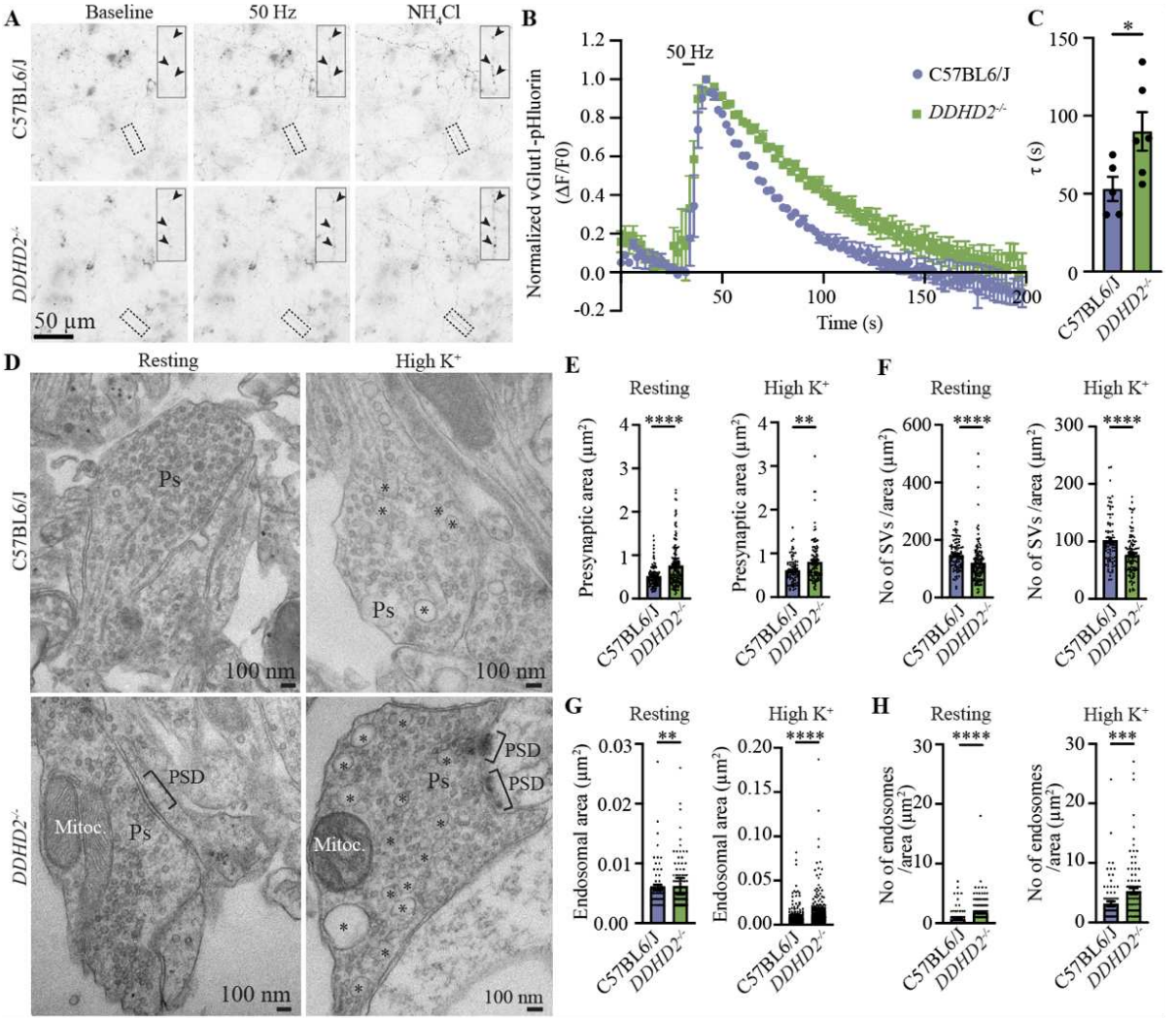

Figure 4. Loss of DDHD2 leads to perturbed synaptic vesicle recycling. (A) Representative images of C57BL6/J and *DDHD2*$^{-/-}$ hippocampal neurons expressing vGlut1-pHluorin in resting (baseline), following stimulated with a train of 300 action potentials (50 Hz, 6 s), and NH_4Cl dequenching. Boxed areas are magnified in the insets and arrowheads indicate presynapses. (B) Averaged, normalized vGlut1-pHluorin traces ($\Delta F/F_0$) from C57BL6/J and *DDHD2*$^{-/-}$ hippocampal neurons stimulated with a train of 300 action potentials (50 Hz, 6 s). (C) Comparison of endocytosis time-constant (τ) values in C57BL6/J (N = 4 neurons) and *DDHD2*$^{-/-}$ hippocampal neurons (N = 5 neurons) from three independent cultures. Results are presented as mean ± sem, student's t test, $*p < 0.05$. (D) Representative electron microscopy (EM) images of cultured E16 C57BL6/J and *DDHD2*$^{-/-}$ hippocampal neuron (DIV21-22) presynapses (Ps) in resting (non-stimulated) condition and following a 5 min high K^+ stimulation. Endosomes (asterisks), mitochondria (Mitoc.), and postsynaptic density (PSD) are indicated. Quantification of (E) presynaptic area (µm^2), (F) number of synaptic vesicles per presynaptic area (µm^2), (G) endosome area (µm^2), and (H) number of endosomes per presynaptic area (µm^2) in cultured C57BL6/J and *DDHD2*$^{-/-}$ hippocampal neurons in resting (non-stimulated) condition and following a 5 min high K^+ stimulation. EM images were obtained from 80-90 nm thin sections and results are shown as mean ± sem, student's t test, $**p<0.01$, $***p<0.001$, $****p<0.0001$, N = 3 independent experiments in each condition.

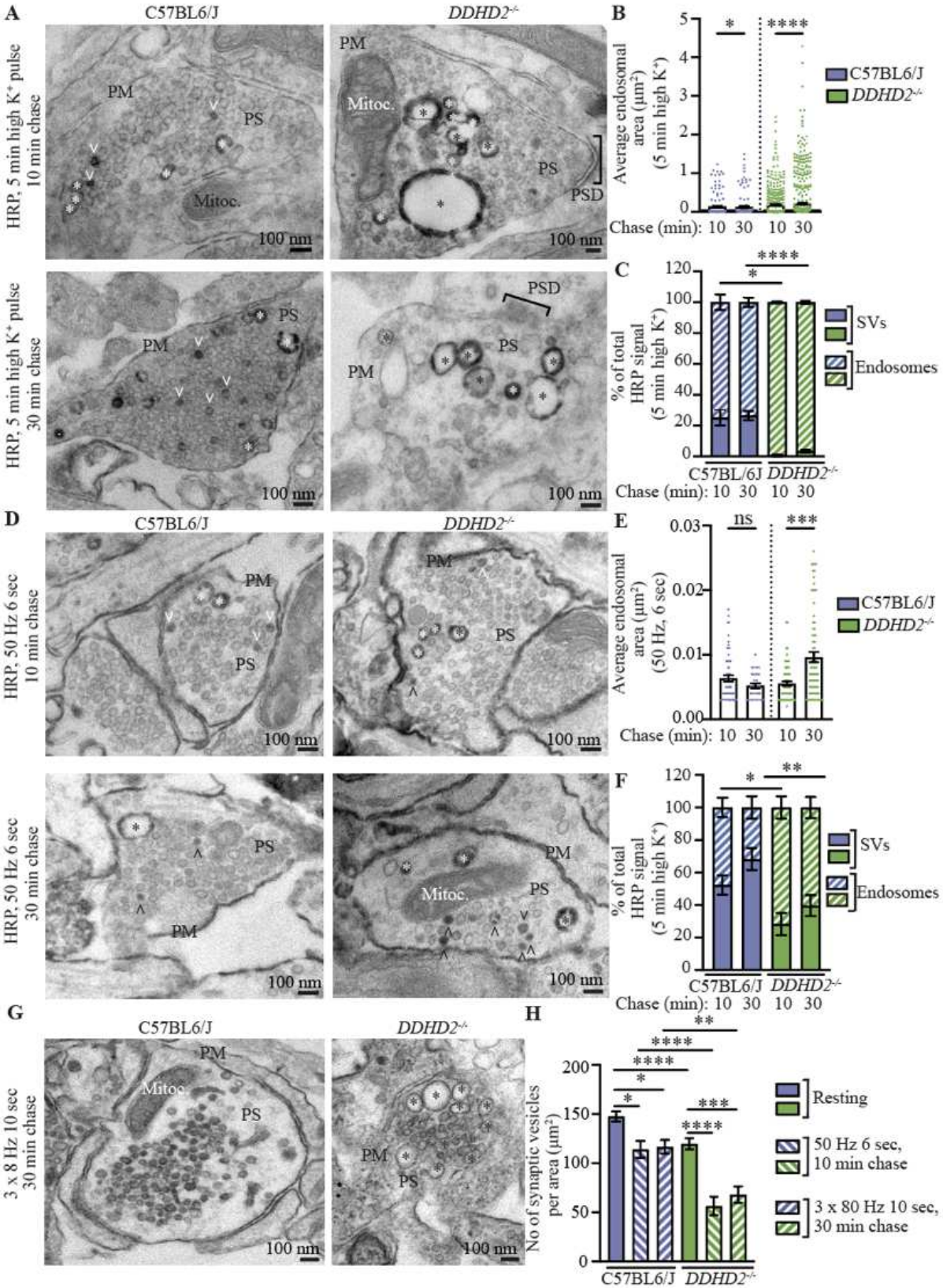

Figure 5. Loss of DDHD2 leads to a perturbed balance between synaptic vesicle recycling and activity dependent bulk endocytosis. (A) Representative electron microscopy (EM) images of cultured E16 C57BL6/J and *DDHD2*$^{-/-}$ hippocampal neuron (DIV21-22) presynapses (Ps) following a 5 min pulse with high K+ buffer in the presence of horse radish peroxidase (HRP) and either 10 min or 30 min chase at 37C in cell culture incubator, after which the neurons were fixed, and cytochemically stained (electron dense dark precipitate) and processed

for EM. Endosomes (asterisks), synaptic vesicles (open arrowheads), plasma membrane (PM), mitochondria (Mitoc.), and postsynaptic density (PSD) are indicated. Quantification of (B) average endosome area (μm^2) and (C) % of total HRP-stained synaptic vesicles (SVs) and endosomes in indicated conditions from cultured C57BL6/J and *DDHD2*$^{-/-}$ hippocampal neurons. Results shown as average ± sem, Kruskal-Wallis multiple comparisons test, *p<0.05, ****p<0.0001, N = 3 independent experiments in each condition. (D) Representative EM images and quantification of (E) average endosome area (μm^2) and (F) % of total HRP-stained synaptic vesicles (SVs) and endosomes in indicated conditions from cultured C57BL6/J and *DDHD2*$^{-/-}$ hippocampal neuron (DIV21-22) presynapses (Ps) following a stimulation with a train of 300 action potentials (50 Hz, 6 s) in the presence of HRP, and either 10 min or 30 min chase at 37C in cell culture incubator, after which the neurons were fixed, and cytochemically stained (electron dense dark precipitate) and processed for EM. Endosomes (asterisks), synaptic vesicles (open arrowheads), plasma membrane (PM), mitochondria (Mitoc.), and postsynaptic density (PSD) are indicated. Results shown as average ± sem, Kruskal-Wallis multiple comparisons test, ns, non-significant, *p<0.05, **p<0.01, ***p<0.001, N=1 independent experiment in each condition. (G) Representative EM images and quantification of (H) number of synaptic vesicles per presynaptic area (μm^2) in resting (non-stimulated) and following a stimulation with a train of 300 action potentials (50 Hz, 6 s), or 800 action potentials repeated three times (3x80 Hz, 10 s) and either 10 min or 30 min chase in cultured C57BL6/J and *DDHD2*$^{-/-}$ hippocampal neurons. Endosomes (asterisks), plasma membrane (PM), and mitochondria (Mitoc.) are indicated. Results shown as average ± sem, Kruskal-Wallis multiple comparisons test, *p<0.05, **p<0.01, ***p<0.001, ****p<0.0001, N = 1-3 independent experiments in each condition.

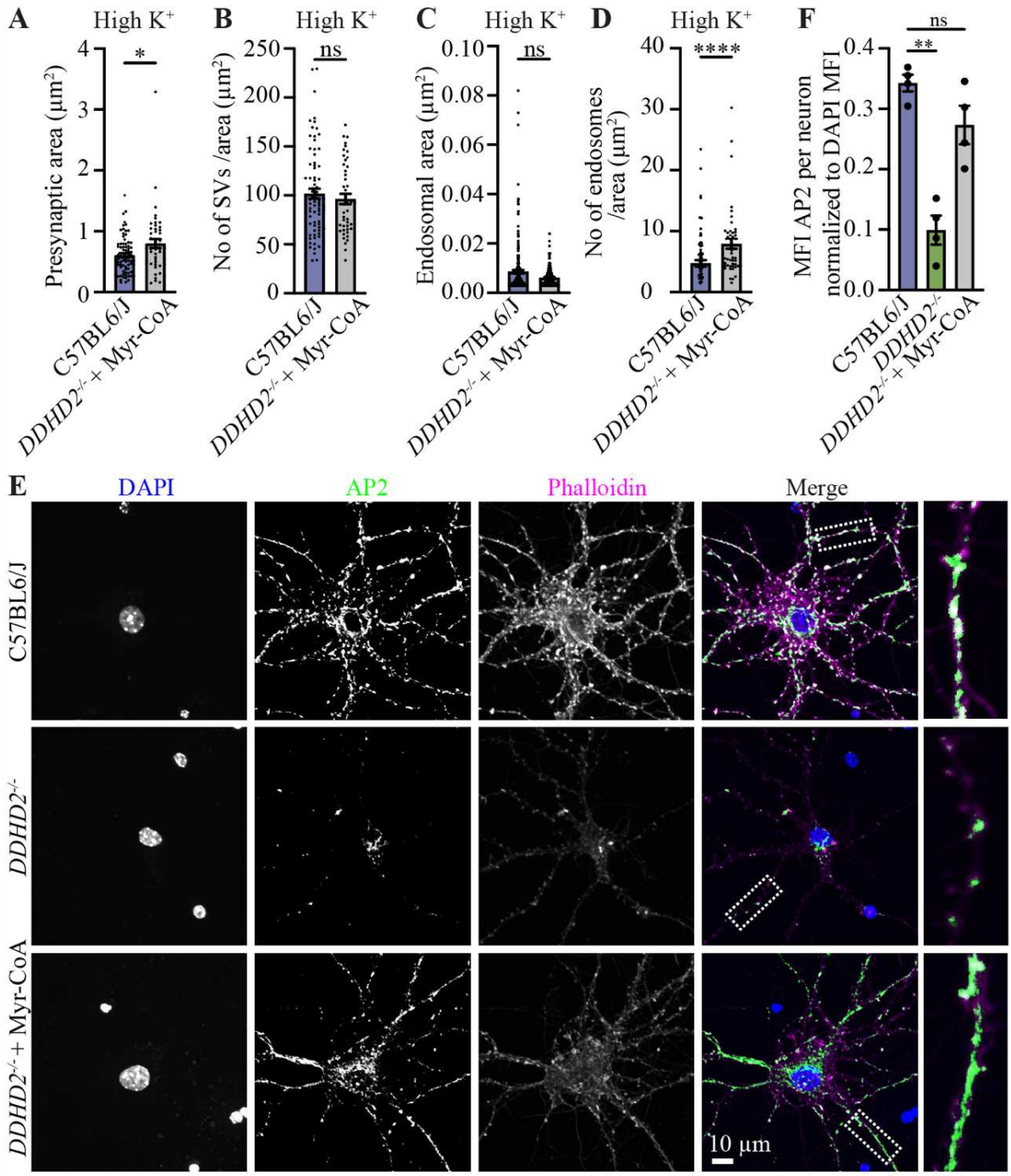

Figure 6. Activity-dependent synaptic vesicle recycling defects and mislocalization of clathrin adaptor AP2 associated with the loss of DDHD2 is significantly rescued with Myr-CoA supplementation. Quantification of (A) presynaptic area (µm^2), (B) number of synaptic vesicles per presynaptic area (µm^2) (C) endosome area (µm^2), and (D) number of endosomes per presynaptic area (µm^2) in cultured C57BL6/J, and *DDHD2*$^{-/-}$ hippocampal neurons rescued with 1 µM Myr-CoA for 16 hours, following a 5 min high K$^+$ stimulation, fixation, and preparation for EM. Results shown as average ± sem, student's t test, ns, non-significant, *p<0.05, ****p<0.0001, N = 3 independent experiments in each condition. (E) Representative maximum projection confocal images of cultured E16 C57BL6/J and *DDHD2*$^{-/-}$ hippocampal neurons (DIV21-22), as well as *DDHD2*$^{-/-}$ hippocampal neurons treated with 1 µM Myr-CoA for 48 h, and immunostained for endogenous AP2 (green). DAPI (nucleus, blue) and Phalloidin (actin, magenta) staining are shown for reference. Boxed areas are shown magnified on right.

(F) Quantification of mean fluorescent intensity (MFI) of AP2 per neuron, normalized to DAPI MFI in indicated conditions. Results shown as average ± sem, Kruskal-Wallis multiple comparisons test, ns, non-significant, **$p<0.01$, N = 3 independent experiments in each condition.

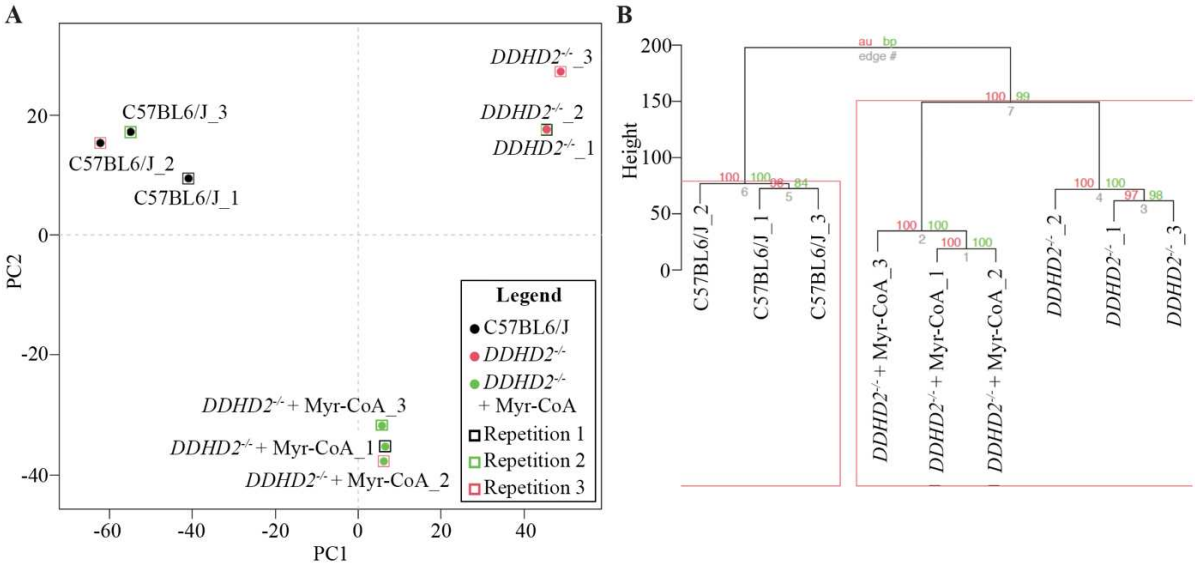

Supplemental Figure 1. Mass spectrometry analysis of C57BL6/J, *DDHD2*$^{-/-}$ and *DDHD2*$^{-/-}$ treated with 1 µM Myr-CoA for 48 h. (A) Principle component analysis. The first two principle components that explained the most amount of variation are shown (x and y-axis). Samples can be observed to cluster according to their experimental group. (B) Hierarchical clustering. Samples cluster according to their experimental group (within each of the tree-like - dendrograms). Values on branches and the red box, represent probabilities of observing the clustering after 100 bootstraps. N = 3 independent experiments in each group.

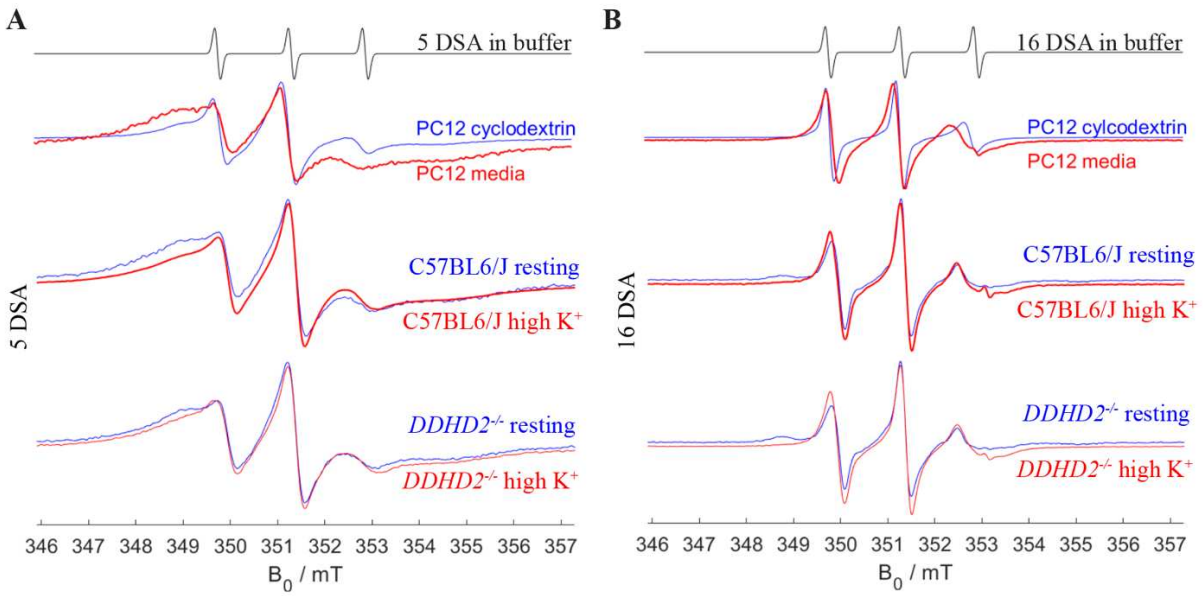

Supplemental Figure 2. Loss of DDHD2 function does not alter neuronal plasma membrane fluidity. X-band (9.852) CW EPR spectra recorded from E16 C57BL6/J and *DDHD2*$^{-/-}$ neurons at DIV21-22 in resting condition (non-stimulated) and following high K^+ stimulation at room temperature using a microwave power of 16 mW and a modulation amplitude of (A) 0.3 mT (DSA5) and (B) 0.1 mT (DSA16). PC12 neurosecretory cells treated with cyclodextrin or DMSO (vehicle media) are shown as a positive control, increasing the membrane fluidity. N = 3 independent experiments in each condition.